Journal of Natural Products
Vol. 47, No. 2, pp. 226-259, Mar-Apr 1984

RECENT DEVELOPMENTS IN ^{13}C- AND PROTON-NMR[1]

JAMES N. SHOOLERY

NMR Applications Laboratory, Varian Associates, P.O. Box 10800, Palo Alto, CA 94303

ABSTRACT.—The fundamentals of pulsed Fourier transform NMR and nuclear spin dynamics are reviewed as a basis for explaining several recently developed experiments: APT, INEPT, carbon-carbon connectivity, and a number of two-dimensional versions of these basic pulse sequences. The general procedures for applying these experiments are outlined and examples of the results are given. The direct evidence of chemical bonding provided by these methods offers a more reliable procedure for structural determinations than traditional inferential methods based on spectral interpretation. Application of these techniques to natural product structure elucidation is illustrated by several examples.

The revolutionary changes that occurred in nmr during the 1970s have continued into the 1980s at an accelerating rate. Improvements in superconducting magnet technology, instrumentation, data processing, and associated techniques are profoundly changing the way in which chemists are solving structural problems.

Most organic chemists are probably aware that modern instruments can provide proton nmr spectra from sub-milligram samples of complex substances quickly and easily. Unfortunately, the progress made in improving ^{13}C-sensitivity is not so widely appreciated. This is not surprising because carbon-13 is only 1.1 percent abundant, and, with a magnetic moment nearly four times smaller than that of the proton, it is intrinsically 62.5 times harder to detect. The product of these two factors results in an overall sensitivity that is 5700 times less than for protons. However, these seemingly insurmountable problems are more apparent than real.

With current nmr instrumentation, the ^{13}C-nuclei in a 1.0 mg sample of cholesteryl acetate give a very informative spectrum after 10 min of data acquisition. Figure 1 shows that each carbon in the molecule gives a resolvable peak in the ^{13}C-nmr spectrum.

It is possible to determine the number of carbons in an unknown natural product structure by direct observation of the ^{13}C-spectral peaks, but this information alone is not very useful. The use of broadband decoupling usually allows the number of singly bonded, doubly bonded, and carbonyl carbons to be determined from the chemical shifts of the ^{13}C-peaks. As shown in Figure 1, irradiation of the protons at their nmr precession frequencies effectively eliminates their spin-spin coupling to the ^{13}C-nuclei, simplifying the spectrum and improving sensitivity by collapsing the multiplets to single lines. But, under these conditions, all ^{13}C-peaks look alike, and the number of protons bonded to each carbon cannot be determined.

Turning off the proton decoupler during data acquisition solves the problem of eliminating the proton couplings but creates so many other problems that it is rarely the preferred method. A better method is to leave the proton decoupler turned on and to move its frequency to an "off-resonance" position, usually 1 or 2 KHz away from the center of the proton spectrum. The ^{13}C-signal enhancement due to the nuclear Overhauser effect (nOe) is preserved, and the CH coupling constants are "reduced." However, the reduced coupling patterns still exhibit so much overlap that only a few of the carbons in Figure 1 can be assigned with confidence. Fortunately, new experiments have been devised that take advantage of some unique properties of pulsed Fourier Transform nmr and provide satisfactory solutions to this problem.

[1]Presented as a plenary lecture at the "Recent Developments in NMR and Mass Spectral Analysis of Natural Substances" Symposium of the 24th Annual Meeting of the American Society of Pharmacognosy at the University of Mississippi, Oxford, MS, July 24-28, 1983.

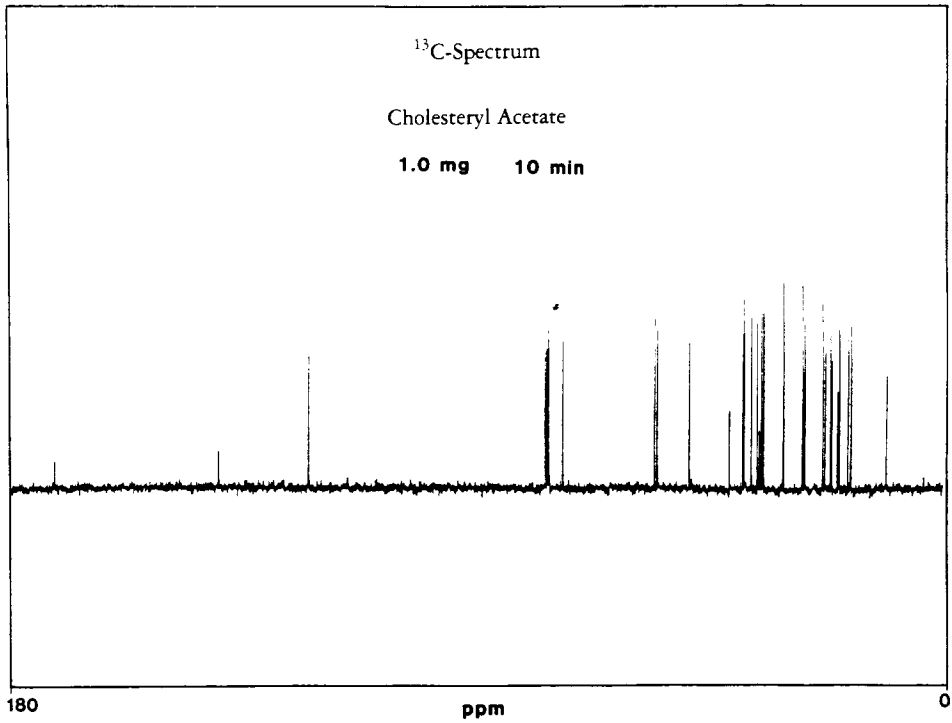

FIGURE 1. Broadband decoupled ^{13}C-nmr spectrum of 1.0 mg of cholesteryl acetate at 100 MHz.

PULSED FOURIER TRANSFORM NMR.—Modern nmr spectrometers operate in a pulsed mode, irradiating the nuclei whose precession frequencies (chemical shifts) are to be observed with an intense radio-frequency pulse lasting only a few microseconds. During this pulse, all of the nuclei are reoriented in the magnetic field and, at the end of the pulse, are left in a nonequilibrium state. In the interim between pulses, the nuclei precess at frequencies that depend upon whatever chemical shifts and spin-spin couplings are influencing them. The precessing magnetization gradually disappears due to various relaxation processes.

The precession of each ensemble of chemically equivalent nuclei causes an exponentially decaying sinusoidal voltage in the receiver coil surrounding the sample. The superposition of all of these waveforms is a complex, time-dependent voltage called the "free induction decay" (FID). Because the FID is just a sum of decreasing sine waves of various frequencies, Fourier Transformation (FT) is able to sort out those frequencies and represent them as a "spectrum" of lines on a frequency scale, namely, the nmr spectrum.

A major advantage of pulsed FT nmr that is just beginning to be appreciated arises from separation in time of the nuclear excitation and subsequent detection of the precession frequencies. In fact, detection can occur at any time after the pulse, although the longer the delay in acquiring the data, the weaker the signals will be relative to the constant noise of the detector. Because both protons and ^{13}C-nuclei in small and medium-sized molecules have relaxation times of the order of seconds, various interactions between the nuclei can be allowed to "evolve" before detecting the nmr signals. This evolution provides an elegant solution to the problem of determining the number of protons bonded to each carbon atom in a molecule and opens up entirely new possibilities for other selective observation of interactions between magnetic nuclei.

NUCLEAR SPIN DYNAMICS.—The basis of the newer pulsed nmr experiments is

easier to describe using some simple diagrams depicting the motions of the nuclear spin vectors. If the delay between excitation pulses is long enough that all transverse magnetization disappears, just before each pulse, the sample can be represented solely by a static magnetization, M_0. As shown in Figure 2a, M_0 lies parallel to the strong magnetic field, H_0, along the z-axis of a Cartesian coordinate system. This vector, M_0, is the sum of all of the magnetic moment vectors of the individual nuclei aligned parallel to the field, minus all of the magnetic moment vectors aligned antiparallel to the field. The population difference follows a Boltzmann distribution and amounts to about one in every hundred thousand magnetic nuclei contributing to the equilibrium magnetization, M_0.

If, in some magical way, the magnetic field could suddenly be shifted 90° from its original direction, (*e.g.*, along the y-axis) the nuclei would no longer be in equilibrium. By convention, the axes are relabeled so that the strong field is again in the z-direction, but the nuclear magnetization would be found along the y-axis, and designated M_y. Nuclei behave like small gyroscopes because of their spin angular momentum, and under the influence of the force trying to align them with the strong field, M_0, they would precess around the z-axis at the angular velocity $\omega=\gamma H$ as shown in Figure 2b. The constant, γ, is called the magnetogyric ratio of the nucleus, and H is the actual value of the field at the nucleus, slightly different for each chemically shifted site in the molecule.

After precession is allowed to continue for a time, t, a sample containing nuclei in chemically nonequivalent sites would no longer be represented by a single static magnetization vector. At an instant t, the magnetization would be separated into vectors

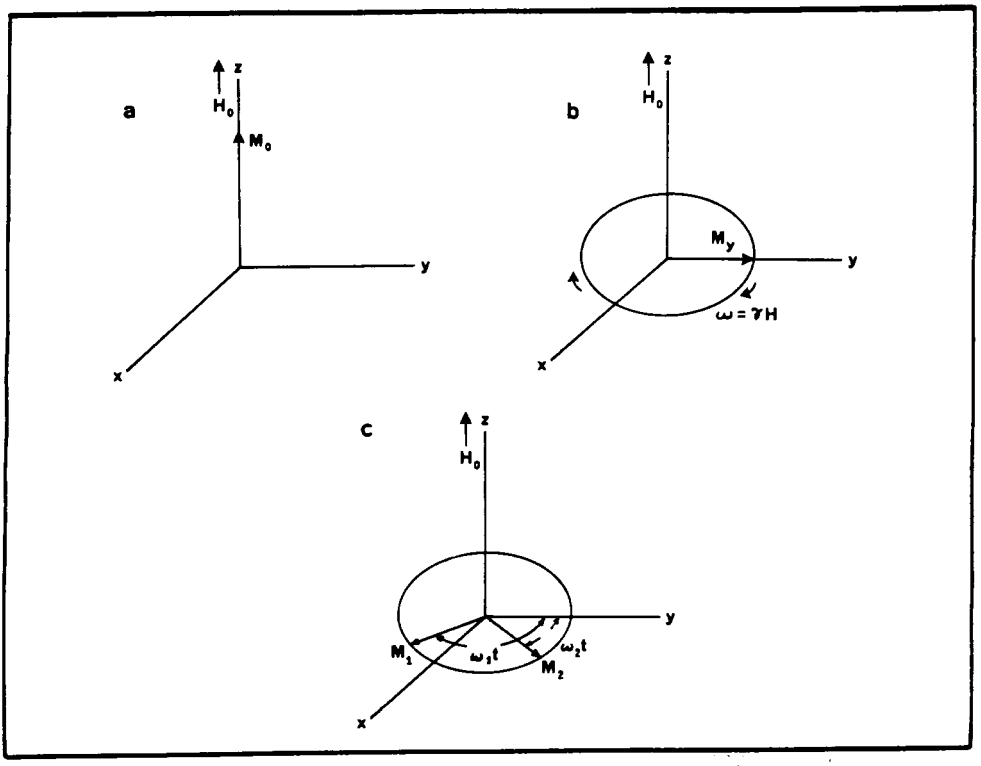

FIGURE 2a. Equilibrium magnetization representing the magnetic moment of the excess nuclear spins aligned parallel to a strong magnetic field, H_0.

FIGURE 2b. Precession of the magnetization around the magnetic field.

FIGURE 2c. Separation of the magnetization associated with two groups of nuclei with different chemical shifts.

that have precessed through different angles, for example, $\omega_1 t$ and $\omega_2 t$, as illustrated in Figure 2c.

Now imagine that, instead of a static Cartesian coordinate system, the coordinate system is rotating at the same angular velocity, ω_0, as the reference line in the spectrum. For protons or ^{13}C, this is the precession frequency of tetramethylsilene (TMS) in the magnetic field of the spectrometer. In such a rotating coordinate system, the TMS magnetization would appear to be a constant vector along the y-axis. The lines in the spectrum that precess at slightly higher frequencies would move clockwise in the rotating frame at the rate $(\omega_i-\omega_0)$, where this term is just the frequency difference between spectral line, i, and the TMS referernce line. These frequencies are, at most, a few thousand Hertz.

In the rotating coordinate system, the nuclei would appear either to stand still or to precess slowly. This corresponds to an effective field along the z-axis of either zero or some small value. Thus, in the rotating frame, the strong, static magnetic field, H_0, essentially vanishes, and the effect of much weaker magnetic fields upon the nuclei can be easily observed. These weaker magnetic fields would have to be rotating at the frequency of the nuclei in order to exert a constant force. Such a rotating field, H_1, would be represented as a static vector in the rotating frame of reference.[2]

THE EFFECT OF A RADIO FREQUENCY PULSE.—A rotating magnetic field can be applied to the nuclei by a coil of wire around the x-axis of the laboratory coordinate system. If energized by an oscillating current at the reference frequency, ω_0, the coil provides what appears to the nuclei to be a static magnetic field, H_1, in the rotating frame of reference. From the instant it is switched on, it is the only field seen by the nuclear magnetization, M_0. Therefore, M_0 precesses at a rate $\omega=\gamma H_1$ in the zy plane as shown in Figure 3a. In the case of ^{13}C-nuclei, a rotating magnetic field strength of 10 gauss would result in one full rotation of M_0 from $+z$ to y to $-z$ to $-y$ and back to the original $+z$ direction in 100 microseconds.

If, instead, a pulse of radio-frequency energy applies a 10-gauss H_1 field for 25 microseconds, the vector M_0 will rotate 90° to point along the y-axis, and will proceed no farther. Thus, the exact result gained with the original assumption—that the static magnetic field was magically rotated 90°—can actually be obtained by rotating the nuclei, not the strong static field. The subsequent precession of the nuclei under the influence of the strong field H_0 allows us to measure their chemical shifts and to examine their interactions with one another.

Because the nuclei are reoriented suddenly, in microseconds, they are said to be flipped, and the degree of reorientation is called the flip angle. A pulse that causes a 90° flip is called a 90° pulse, or sometimes a $\pi/2$ pulse. Doubling the pulse length would give a π-pulse, or 180° pulse, and would invert the nuclear magnetism.

If a 90° pulse is applied to a spin system, the full value of the magnetization, M_0, is converted to transverse magnetization, M_y, leaving $M_z=0$. If a second pulse is applied immediately, there is no M_z magnetization to tip into the y-direction, and, consequently, no signal can be acquired as a result of the second pulse. If, however, the pulse is delayed for several times as long as the spin-lattice relaxation time for the nuclei, the magnetization will have reappeared along the z-axis and can again be tipped 90° into the y-direction. During most of this long "recovery" time, no data are acquired. Although this mode of operation is not very efficient, it has advantages for quantitative measurements.

An alternative, often used for qualitative spectral measurements, is to use a small flip angle, for instance 30°, and a more rapid repetition rate. Figure 3b shows that im-

[2]For the purposes of this discussion, it will be assumed that an oscillating current in a coil of wire can generate a magnetic field rotating at the same frequency.

mediately after the 30° pulse, the magnetization not only has a component M_y that is ½ M_0, but also has a component M_z that is $\sqrt{3/2}\,M_0$, or 85% of the original equilibrium magnetization. Although the precessing M_y magnetization generates signals that are only half as large as those from a 90° pulse, the next pulse can be applied as soon as the signal from the first pulse dies away. At a given pulse repetition rate, there is an optimal tip angle that depends upon the relaxation time, and using the optimal tip angle allows more efficient detection of the nmr signals than using 90° pulses and long recovery delays.

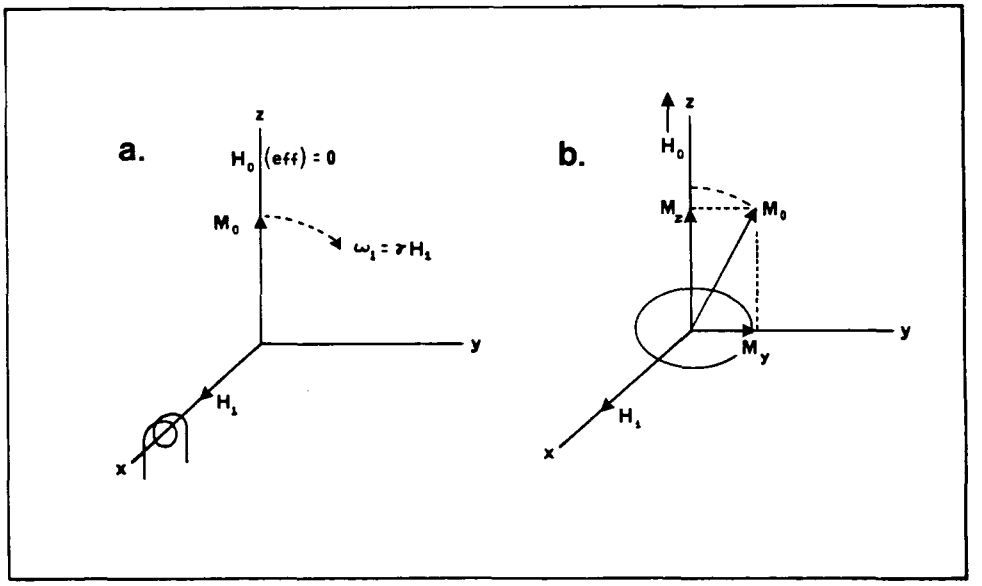

FIGURE 3a. Precession of the equilibrium magnetization around the axis of the radio-frequency field H_1 to a nonequilibrium position in the rotating frame of reference.

FIGURE 3b. Components of magnetization after tipping the equilibrium magnetization 30°.

THE APT EXPERIMENT.—The behavior of the ^{13}C-magnetization after a 90° pulse can be used to overcome the loss of information caused by proton decoupling. For this purpose, an ingenious experiment called APT, an acronym for Attached Proton Test, has been developed (1,2). A ^{13}C-nucleus bonded to a proton, *e.g.*, a CH group in a complex molecule, exhibits the least complicated behavior. Immediately after a 90° pulse, the magnetization of the CH group will lie along the y-axis. If the chemical shift of this group happens to be the same as for the reference compound, TMS, the magnetization will appear not to precess in the rotating frame of reference. Only this case will be considered for the present.

Instead of immediately beginning data acquisition, the receiver remains turned "off" for a time, t, as does the proton decoupler. Now the CH carbon magnetization no longer will precess just at the chemical shift frequency but will split into two lines, separated by J_{CH} Hz at $\omega_0+J/2$ and $\omega_0-J/2$. These two states correspond to half the molecules having protons parallel (α) to the static field and half the molecules with protons aligned antiparallel (β) to the field. At a time, t, following the pulse, the magnetization in the rotating frame will consist of the sum of the two magnetization vectors, one that will appear to move clockwise at $J/2$ Hz, and one that will fall behind and move counterclockwise at the same rate. Because the vectors are diverging, their sum (which is what the receiver would detect if it were turned on) is decreasing with time. At a time $1/2J$ sec, the two vectors would oppose and cancel each other. At a time $1/J$ sec, the two

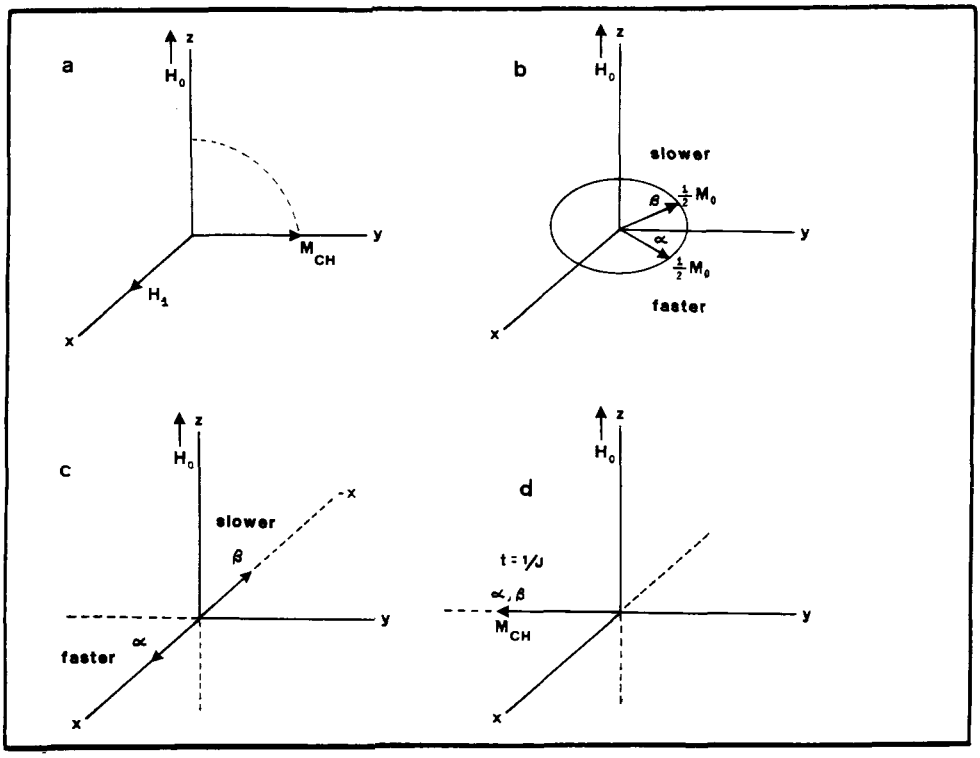

FIGURE 4a. Magnetization of a CH group tipped by a 90° pulse to a position along the y-axis of the rotating frame.

FIGURE 4b. Divergence of the ^{13}C-magnetization vectors associated with proton spin states α and β after short time.

FIGURE 4c. Opposition of magnetization vectors at $t = 1/2J$.

FIGURE 4d. Convergence of magnetization vectors with negative phase at $t = 1/J$.

vectors would be found along the $-$y axis. Figure 4 shows the behavior of M_{CH} from $t=0$ to $t=1/J$.

At the time $1/J$, both the decoupler and the receiver are turned on. The two lines again collapse to a single line with a chemical shift that falls at the reference position in the spectrum. The detected nmr signal is found to have reversed phase, however, and is displayed as a negative peak in the spectrum. The effect of this experiment is, therefore, to reverse the phase of CH carbons, by delaying acquisition $1/J$ seconds with the decoupler turned off.

The behavior of a carbon with two attached protons, a CH_2 group, is different under the conditions of the APT experiment. There are three spin states for the protons: $\alpha\alpha$, $\alpha\beta$ or $\beta\alpha$, and $\beta\beta$, giving a triplet with intensities 1:2:1 for the ^{13}C-spectral line. Figure 5 shows that, after a 90° pulse, these three magnetization vectors are found along the y-axis. The center line precesses at the chemical shift frequency, again taken as equal to the reference frequency, and therefore is a static vector in the rotating frame of reference. The outer lines of the triplet, $\alpha\alpha$ and $\beta\beta$, precess at ω_0+J and ω_0-J, with the result that at the time $1/J$ they will each have completed a full revolution and have rejoined the center line. Detection at this time results in a signal with the normal phase, in contrast to the reversed phase of a carbon with only one attached proton.

A similar analysis shows that a carbon with three attached protons, a CH_3 group, will reverse phase as in the case of a CH carbon, while a nonprotonated carbon, having no CH coupling, will always exhibit a normal phase. The APT experiment thus sorts

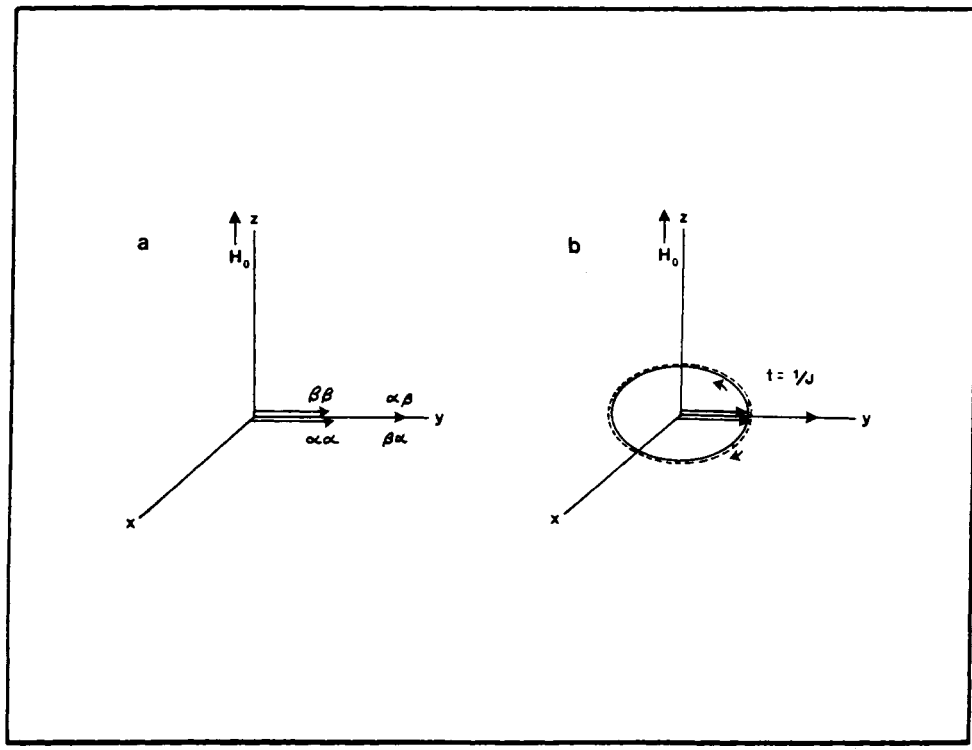

FIGURE 5a. Magnetization vectors of a CH_2 group after a 90° pulse.
FIGURE 5b. Convergence of vectors with normal phase after $t = 1/J$.

the carbons into two types—those with an even number of attached protons and those with an odd number.

A fatal problem exists with this experiment as proposed above. Suppose that the chemical shift of the carbon is not equal to the reference frequency but differs from it by an arbitrary amount, $\omega_0\delta$. Then, in addition to the divergence of the lines of the multiplet, their average position will precess clockwise so that at a time $1/J$, the vectors will merge, but along an axis with a phase shift of $\omega_0\delta/J$. Figure 6 shows that, depending on the value of δ, the signal could have a variable-phase error. The spin-coupling informa-

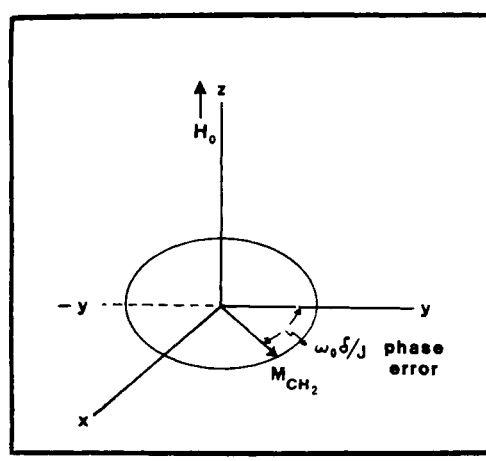

FIGURE 6. Phase error due to precession through the angle $\omega_0\delta/J$ at the time $t = 1/J$.

tion and the chemical shift information are scrambled together, and the experiment cannot be interpreted in a simple way.

Fortunately, a solution to this problem is available. It depends upon the refocusing effect of a 180° pulse applied to nuclear magnetization precessing in the x-y plane. Consider two ^{13}C-spectral lines with different chemical shifts δ_1 and δ_2. At time t=0 after a 90° pulse, their magnetization will be found along the y-axis. After a time, τ, they will have precessed different distances, at which time a second pulse, this time a 180° pulse, is applied by a coil along the y-axis.[3] This pulse reverses the x-coordinates of the magnetization vectors and, as shown in Figure 7, results in the faster precessing vector δ_2 being moved from a leading to a trailing position relative to the slower precessing vector δ_1.

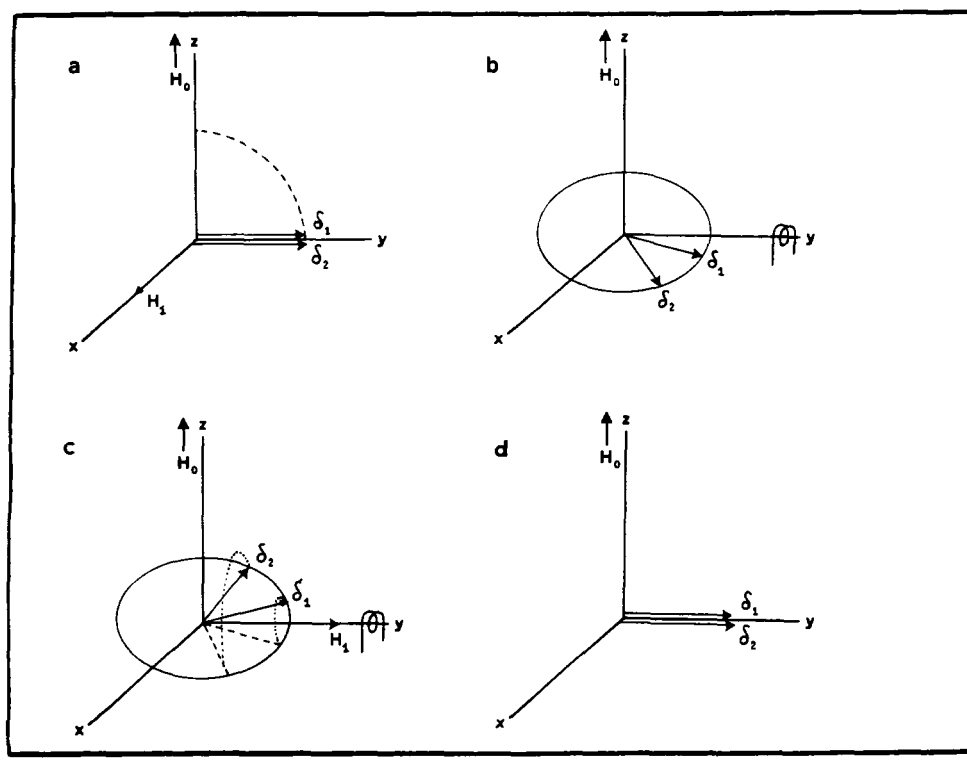

FIGURE 7a. Two magnetization vectors representing nuclei with different chemical shifts after a 90° pulse.
FIGURE 7b. Divergence of the vectors after precession for a time, τ.
FIGURE 7c. Reversal of the x-coordinates of the vectors by a 180° pulse along the y-axis.
FIGURE 7d. Refocusing of the vectors along the y-axis at $t=2\tau$.

By waiting a second time period, τ, exactly equal to the first, both the vectors, δ_1 and δ_2, will be found to have returned at time 2τ to their original position on the y-axis. If we turn on the receiver at this time, the two ^{13}C-spectral lines will be detected with the same phase, *i.e.*, they will both give positive signals exactly as they would if detection had occurred immediately after the original 90° exciting pulse. The signal occurring at time 2τ is called a *spin-echo*, inasmuch as it occurs spontaneously upon the simultaneous refocusing of the various magnetization vectors with different precession rates.

[3]The same result can be achieved with a coil along the x-axis, but with the pulse shifted 90° in phase.

The APT experiment with chemical shift refocusing is represented by the following pulse sequence:

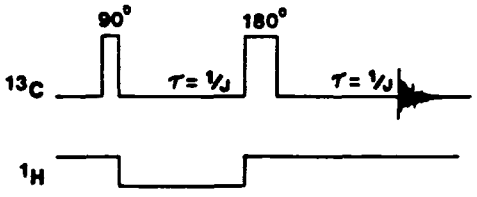

The chemical shift operates during both $1/J$ delay periods and is refocused by the 180° pulse. The divergence of the individual lines of the mutual spin-spin multiplets occurs only during the first $1/J$ delay period; during the second $1/J$ period, the decoupler is turned on, and whatever divergence occurred during the first delay does not refocus. The key to the successful separation of the chemical shift and spin-coupling effects lies in the ability of the spin-decoupler to affect the spin-coupling but not the chemical shift.

The time dependence of the ^{13}C-signals in the APT experiment is shown in Figure 8 for sp^3 carbons ($J_{CH}=125$ Hz) and for sp^2 carbons ($J_{CH}=160$). If the experiment is repeated with the delay set to $1/J$, $1/2J$, and $2/3J$, it is possible to assign all of the spectral peaks. This is illustrated in Figure 9 for cholesterol. The $1/J$ spectrum identifies odd and even numbers of protons. The $1/2J$ spectrum distinguishes the quaternary carbons from the CH_2 carbons, and the $2/3J$ spectrum reduces the CH_3 peaks to about one-third of the intensity of the CH peaks. The great advantage of APT over the off-resonance decoupling method is also illustrated in Figure 9. Only a few of the peaks in Figure 9d can be assigned with confidence.

The selectivity of the APT experiment for protonated and nonprotonated sp^2 carbons makes it extremely useful for clarifying assignments in crowded regions of the ^{13}C-spectrum, where peaks may be accidentally superimposed. Figure 10 shows a

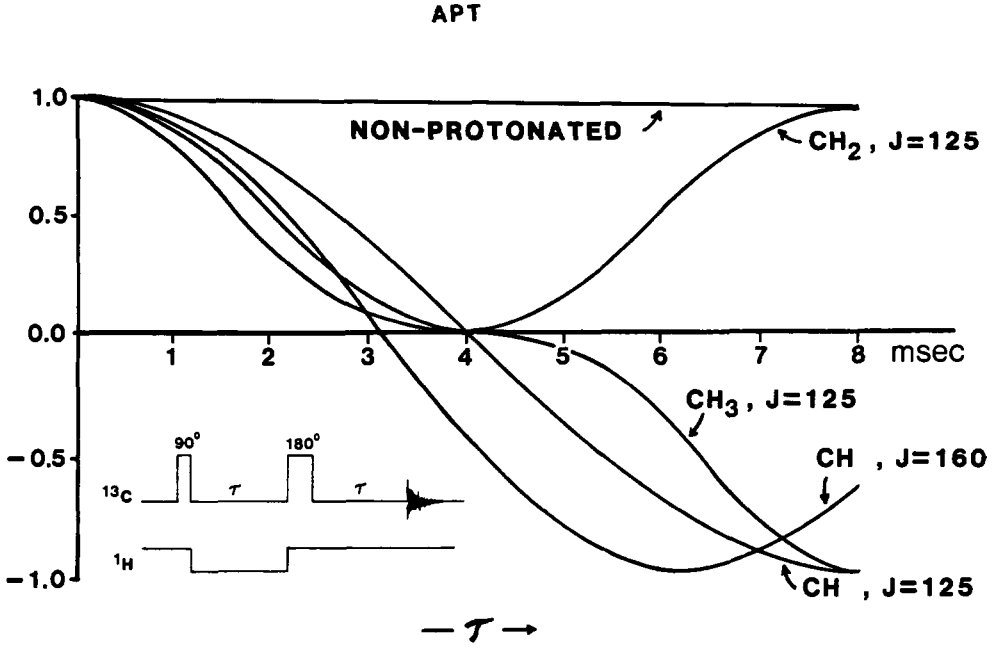

FIGURE 8. Time dependence of signal intensities in the APT experiment.

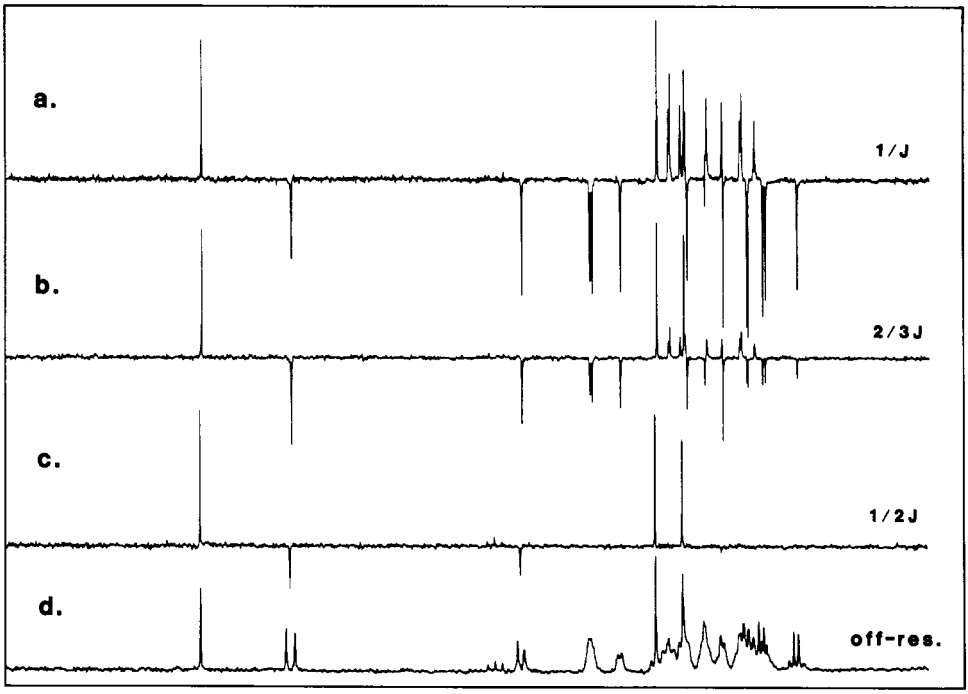

FIGURE 9a. APT spectrum of cholesterol with $\tau = 1/J$.
FIGURE 9b. APT spectrum of cholesterol with $\tau = 2/3J$.
FIGURE 9c. APT spectrum of cholesterol with $\tau = 1/2J$.
FIGURE 9d. Off-resonance CW decoupled spectrum of cholesterol.

molecule with 17 sp^2 carbons, 16 of which should be found between 110 and 160 ppm. Trace **a** shows only 14 peaks. Inverting the protonated carbons ($\tau = 1/2J$) in trace **b** shows eight lines, one of which clearly has an area corresponding to two carbons, so all nine of the protonated carbons are observed. In trace **c**, with $\tau = 1/2J$, the protonated carbons are nulled, revealing that one of the nonprotonated carbon peaks falls exactly on a protonated carbon peak. In trace **c**, all seven of the expected nonprotonated carbon peaks are clearly revealed.

An example of the use of the APT technique in a complex mixture of natural products is illustrated by the analysis of a gas-oil petroleum fraction. As shown in Figure 11, the fraction of aromatic carbons can be measured by integrating the sp^3 and sp^2 regions of the ^{13}C-spectrum. This information is important in characterizing crude petroleum and petroleum fractions, but it gives no insight into the types of aromatic structures that are present. The currently accepted method for determining the relative numbers of protonated and nonprotonated aromatic carbons is based on the assumption that protonated carbons have chemical shifts less than 130 ppm and that nonprotonated carbons have shifts greater than 130 ppm. Figure 12 shows that the ratio of CH/C based on this assumption is 1.39.

Figure 13 shows three measurements of the aromatic carbons. Trace **a** is a spin-echo spectrum with $\tau = 1/J$, but with continuous broadband decoupling, so that all carbon peaks are refocused with the same phase. The integral of trace **a** gives the sum of the protonated and nonprotonated aromatic carbons. Trace **b** shows the result of turning off the decoupler during the first delay period, giving an APT spectrum with the protonated aromatic carbons inverted. The integral of this spectrum must represent the difference of the two aromatic carbon types; namely, the nonprotonated minus the proto-

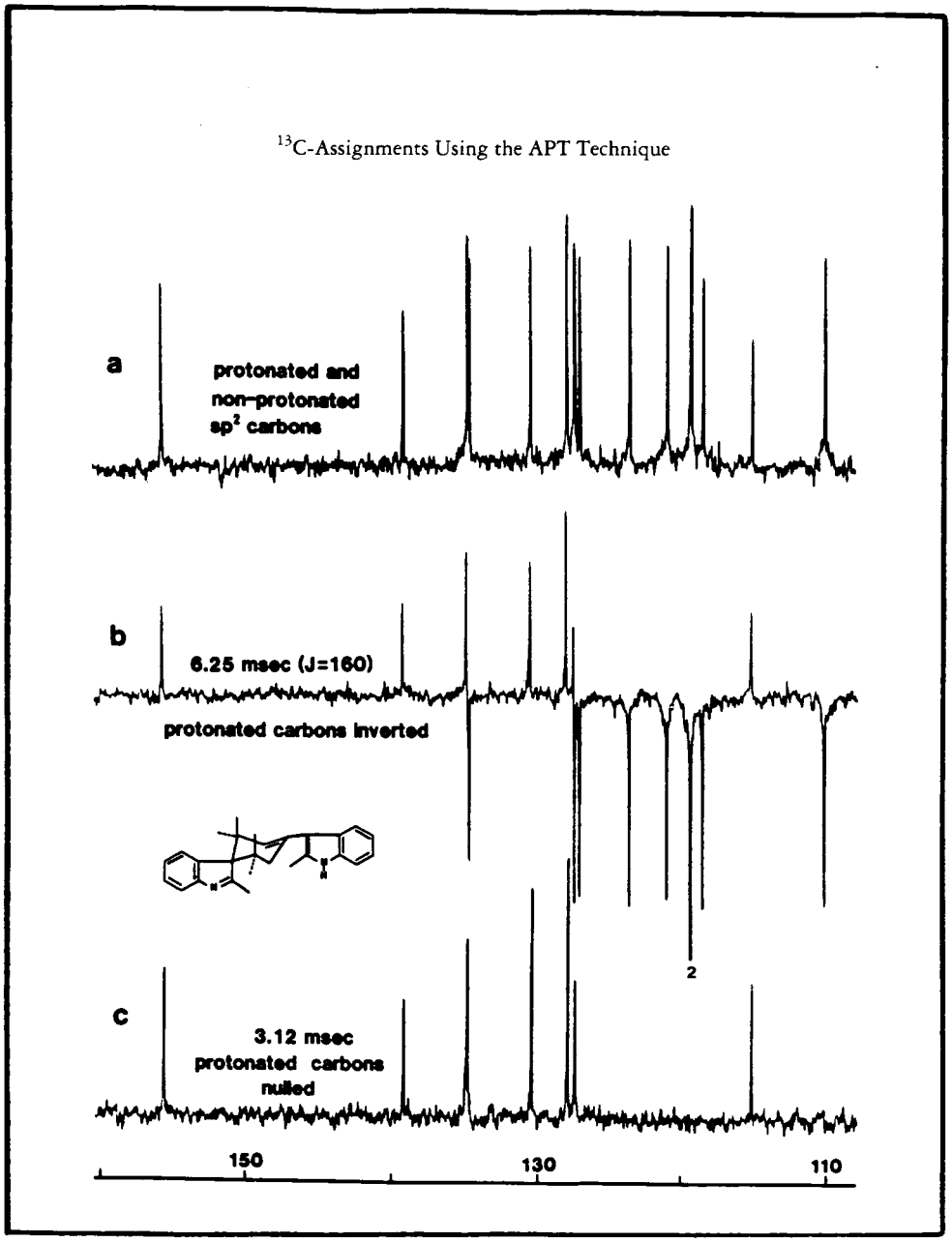

FIGURE 10a. Aromatic carbon spectral region of a complex organic compound.
FIGURE 10b. Protonated aromatic carbons inverted in APT spectrum with $t = 1/J$.
FIGURE 10c. Protonated aromatic carbons nulled in APT spectrum with $t = 1/2J$.

nated aromatic carbons. From these two measurements, the number of both types can be calculated. The ratio of CH/C is found to be 1.68, quite different from the value 1.39 based on the arbitrary assumption of 130 ppm as the dividing line between the CH and C regions. Trace **c** shows the nonprotonated carbons only, since the delay of $1/2J$ nulls the CH signals. The integral of trace **c** agrees well with the value for the nonprotonated carbons calculated from **a** and **b**, and shows that the measurements preserve the quantitative information.

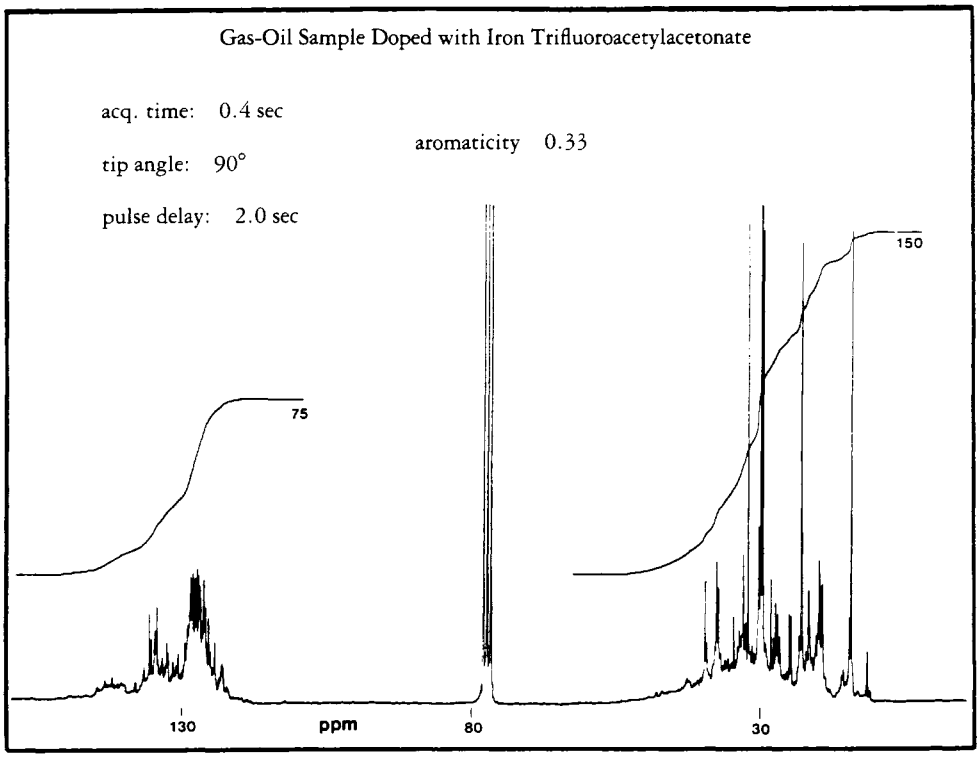

FIGURE 11. ^{13}C-nmr measurement of aliphatic and aromatic carbons in a gas-oil sample.

The APT experiment illustrates a principle that can be utilized in a very powerful class of experiments called two-dimensional (2D) nmr experiments. The principle is that, while the nuclear magnetization is precessing in the x-y plane, internuclear interactions can evolve and alter the phases and amplitudes of the magnetization observed during a subsequent data acquisition period. This is represented schematically as:

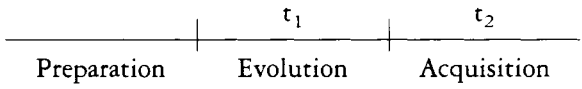

The evolution period and acquisition periods have been designated t_1 and t_2. This is unfortunate, because they bear no relationship to the spin-lattice and spin-spin relaxation times, T_1 and T_2. They simply designate the first and second time periods in the active part of the experiment, *i.e.*, the two time domains of the experiment. The preparation period establishes reproducible starting conditions for the experiment. It may be a passive delay during which the nuclei return to their equilibrium polarization state, or it may include a sequence of pulses to align the nuclear spins in some predetermined way at the instant of initiating the evolution period.

During the time t_1, the x,y, and z components of the magnetization evolve under the influence of all of the forces acting on the nuclei, including the interactions between the spins. The z-component of magnetization existing at the end of t_1 is sampled by a 90° pulse at the observing frequency, and the intensities of the various spectral lines are recorded in the form of a FID during t_2. FT of this FID produces a spectrum of lines in the frequency domain, f_2. They occur at exactly the same frequencies that would be observed in the standard one-dimensional experiment but with intensity variations that depend upon t_1. Figure 14 illustrates this effect for two lines in a proton spectrum as t_1

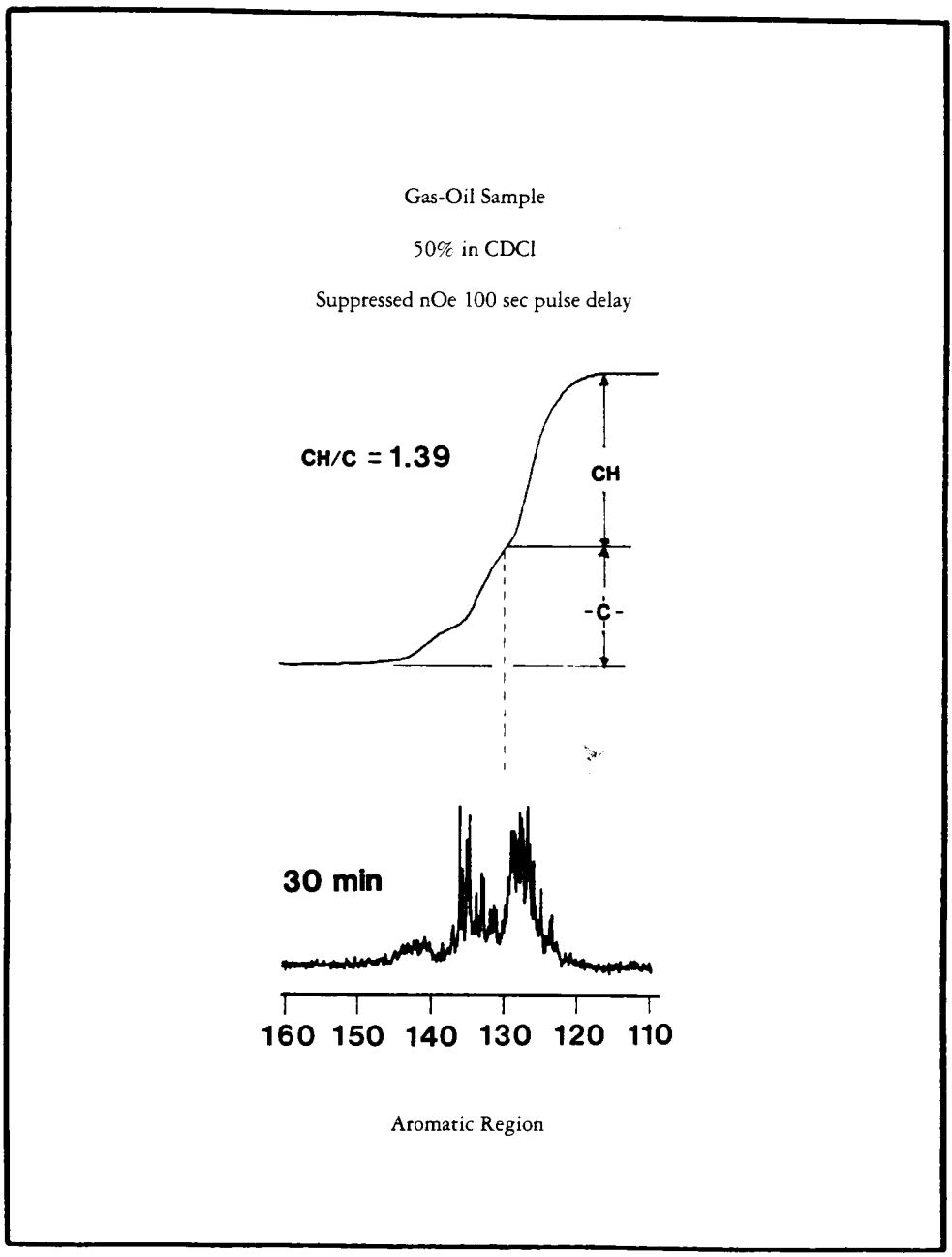

FIGURE 12. Measurement of aromatic CH and nonprotonated aromatic carbons based on separation at 130 ppm.

is varied in 25 increments from zero to ten seconds, while the spins evolve under the influence of a spin-spin coupling of 0.4 Hz. Thus, even weak interactions that are ordinarily difficult to resolve give dramatic intensity variations if allowed to evolve long enough.

The large number of transformed spectra generated from incrementing t_1 can be arranged side by side in a parallel array. This gives each spectral line the appearance of a new FID running at right angles to the spectrum in the frequency domain, f_2. An example, taken from an actual 2D experimental data array, is shown in Figure 15. The inten-

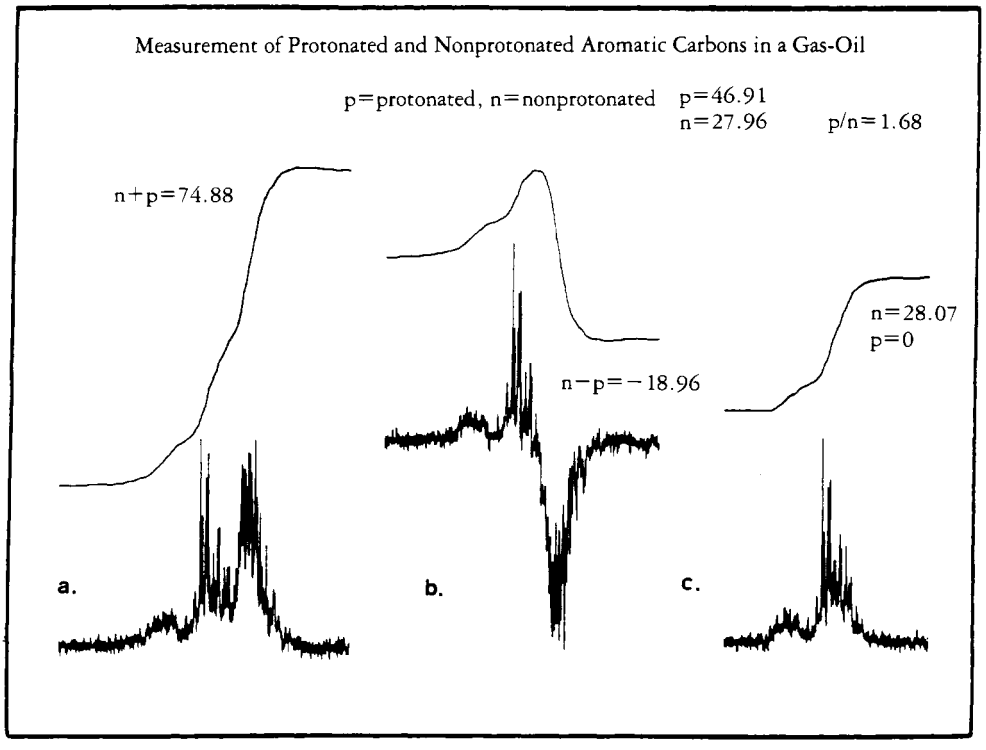

FIGURE 13a. Sum of all aromatic carbons in gas-oil sample.
FIGURE 13b. Difference of aromatic carbons achieved by inverting the protonated aromatic carbon signals
FIGURE 13c. Nonprotonated aromatic carbons achieved by nulling the protonated aromatic carbons.

sity of one carbon peak in coumarin is displayed for each of 512 values of the evolution time. Such a display, called an interferogram, is generated for all of the data points by lining up the f_2 spectra in a parallel array, or data matrix.

The interferograms can be subjected to a second FT. Because the time frame of the interferograms is the t_1 domain, the f_1 domain spectra resulting from the second FT dis-

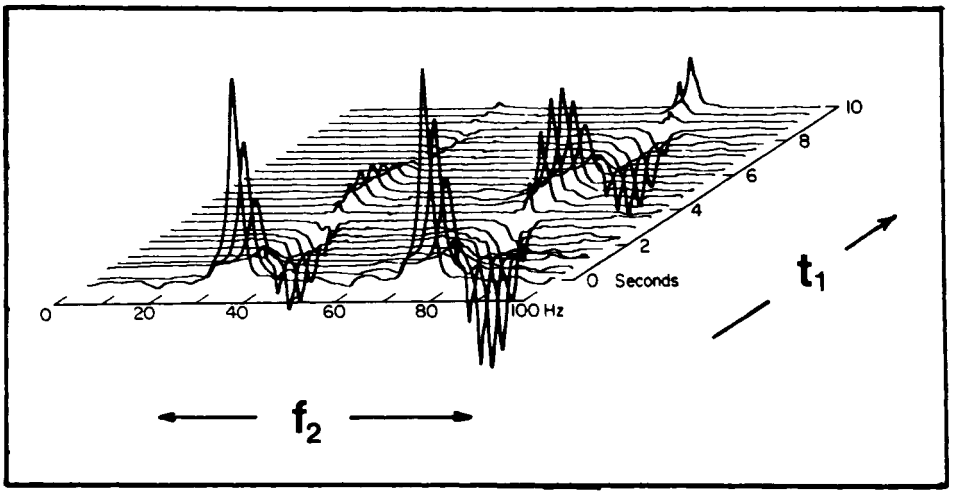

FIGURE 14. Evolution of peak intensities in a spectrum showing two protons with 0.4 Hz spin-spin coupling.

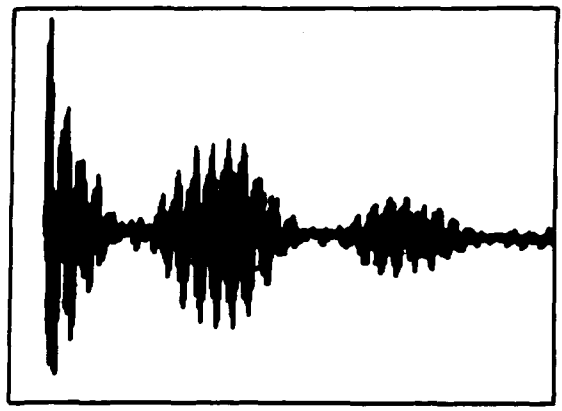

FIGURE 15. The intensity of one spectral peak displayed by lining up 512 spectra with increasing values of the evolution time.

play peaks at positions that depend upon the spin couplings or chemical shifts that evolved during t_1.

A new data matrix can now be generated from a parallel array of all of the f_1 spectra. Peaks appear on a 2D planar surface with the axes f_1 and f_2. Because each point in the 2D array also has an intensity, the full display of the data is three-dimensional.

In all 2D experiments, the f_2 dimension always displays the precession frequencies of the observed nucleus; the f_1 dimension contains information about the frequencies of the interactions between the observed nucleus and other magnetic nuclei that developed during the evolution period.

A perspective view of the 2D array is obtained by making a "stacked" plot, as shown in Figure 16 for the simple four-line quartet from enriched ^{13}C-methyl iodide. The de-

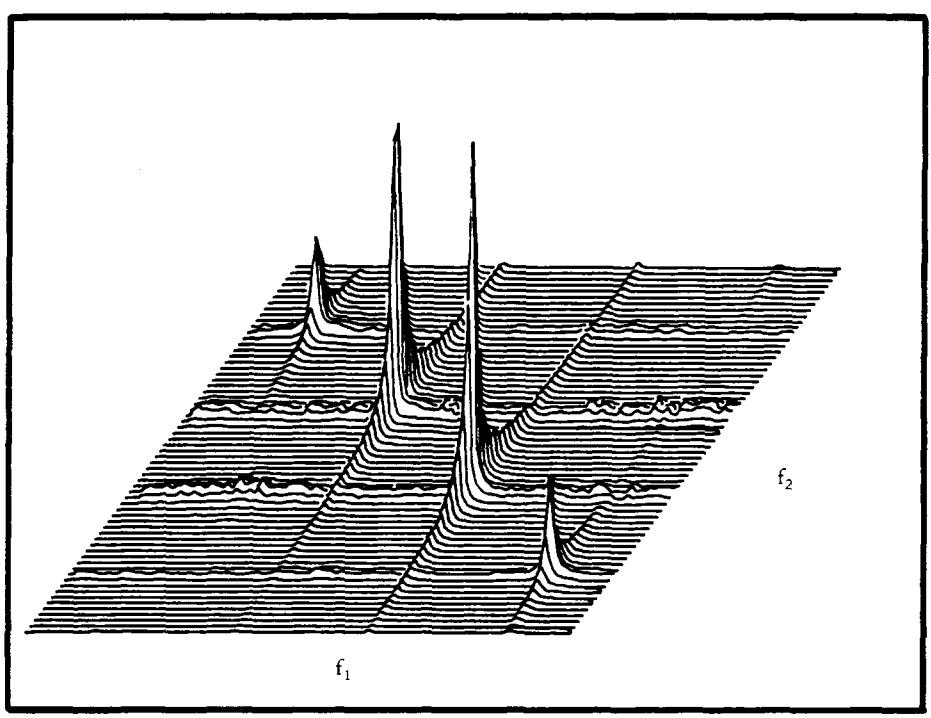

FIGURE 16. Perspective view of a 2D array of peaks.

coupler was off during part of the evolution time and also during the acquisition time. Therefore, the spin-spin coupling of the methyl protons to the ^{13}C appears along both the f_1 and f_2 axes.

HETERONUCLEAR 2D*J* (HET2D*J*) SPECTRA.—In the case of ^{13}C-spectra with broadband proton decoupling during t_2, only the chemical shifts of the carbons appear along the f_2 axis. If the decoupler is turned off during part of the evolution time t_1, the CH couplings appear as frequency shifts along the f_1 axis. By allowing the chemical shift and spin coupling energies to affect the precessing magnetization during different time periods, the overlapping of the coupling patterns found in the normal spectrum is removed.

The pulse sequence used to separate the ^{13}C-chemical shift and the CH spin-spin couplings is just the familiar APT sequence.

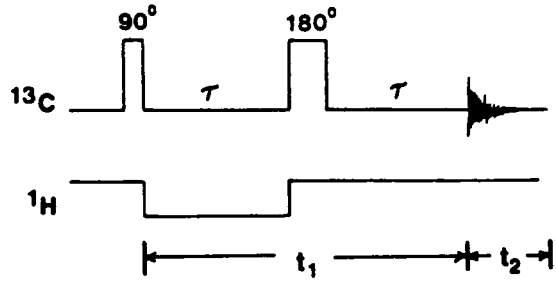

This sequence can be adapted to the 2D mode of operation by taking a large number of spectra, for instance, 256, in which the value of t_1 varies from zero to one second. The intensity of each ^{13}C-spectral line will be modulated at the frequency J_{CH} during the time the decoupler is off, and the 256 measurements of the spectral line intensities will therefore trace out $J/2$ full sinusoidal cycles. When these points are Fourier transformed, the result will be two lines located $\pm J/2$ around the zero frequency in the f_1 dimension. The spectral width in the f_1 dimension determines the maximum value of J_{CH} that can be observed. It is equal to the number of samples taken per second; consequently, in this case couplings up to 256 Hz could be accommodated.

This HET2DJ experiment was used to represent graphically the nonprotonated and protonated aromatic carbons in the gas-oil samples. Figure 17 displays the ^{13}C-chemical shifts along the horizontal axis and offsets the protonated carbon peaks $\pm J/2$ Hz in the J_{CH} dimension. If Figure 17 is viewed from above, the resulting contour plot shows the nonprotonated carbons strung out along the center line of the plot, with the protonated carbons split into two lines displaced ± 80 Hz in the J-dimension, as shown in Figure 18. Horizontal slices of the spectrum are shown in Figure 19 at zero and at ± 80 Hz. The value of their integrals again allows the ratio of protonated to nonprotonated aromatic carbons to be calculated. The result, 1.72, is in good agreement with the result obtained from the one-dimensional experiment.

POLARIZATION TRANSFER.—Spin-spin coupling between protons and ^{13}C-nuclei gives equally spaced doublets in both the proton- and ^{13}C-spectra. Therefore, the number of carbons attached to the protons can be determined simply by applying a 90° pulse at the proton frequency and allowing the proton magnetization vectors to diverge during a free precession period. This reversal of the APT experiment would be pointless, however, because a hydrogen atom can form only one covalent bond, so there is never any question about the number of attached carbons. Also, serious experimental difficulty would arise when the time for detection of the signals arrived, because the signals from the one percent of the protons bonded to carbon-13 would be overwhelmed by the signals from the 99 percent bonded to carbon-12.

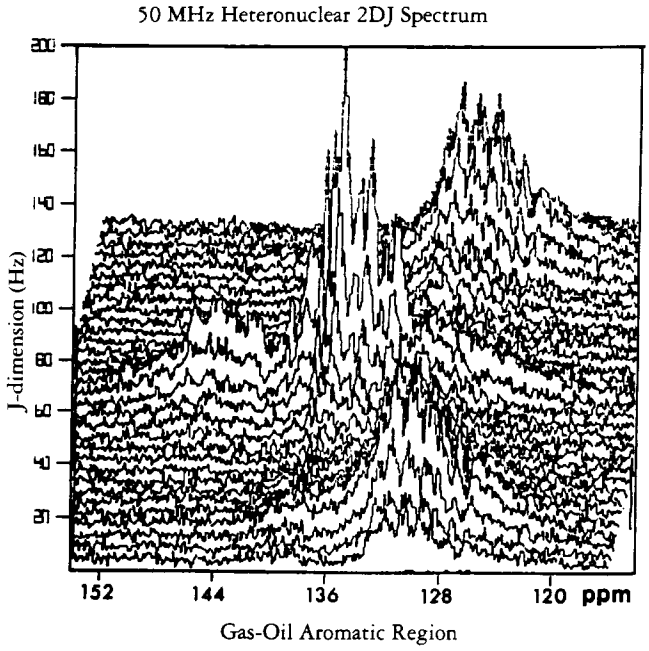

FIGURE 17. Heteronuclear 2D*J* spectrum of the aromatic ^{13}C-region of a gas-oil.

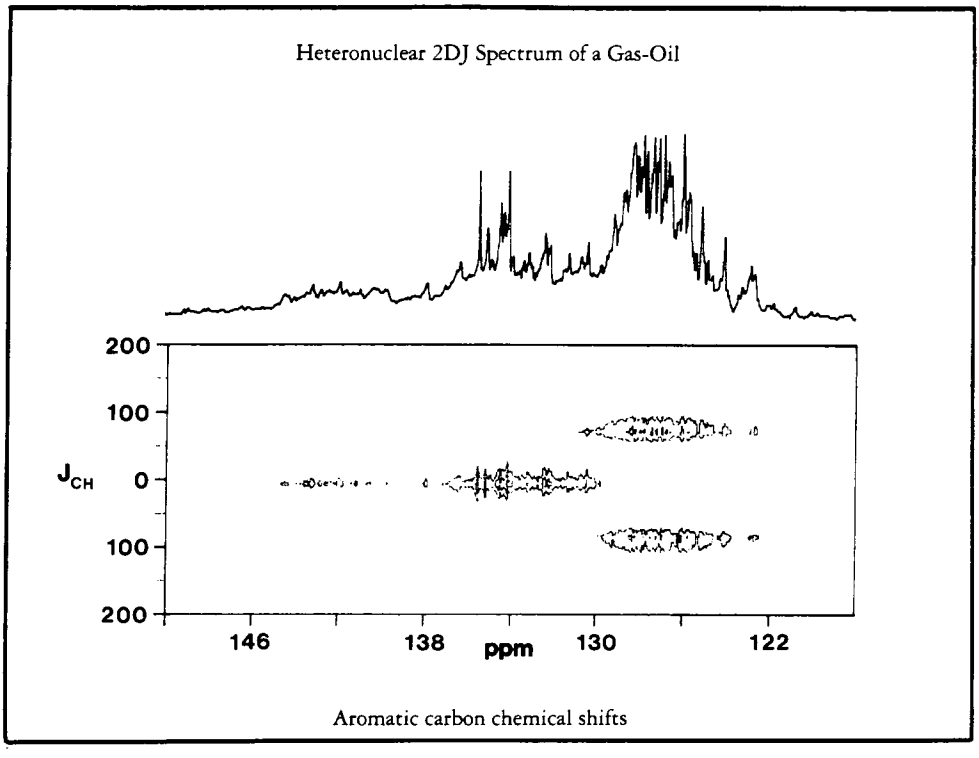

FIGURE 18. Contour plot of the data of Figure 17.

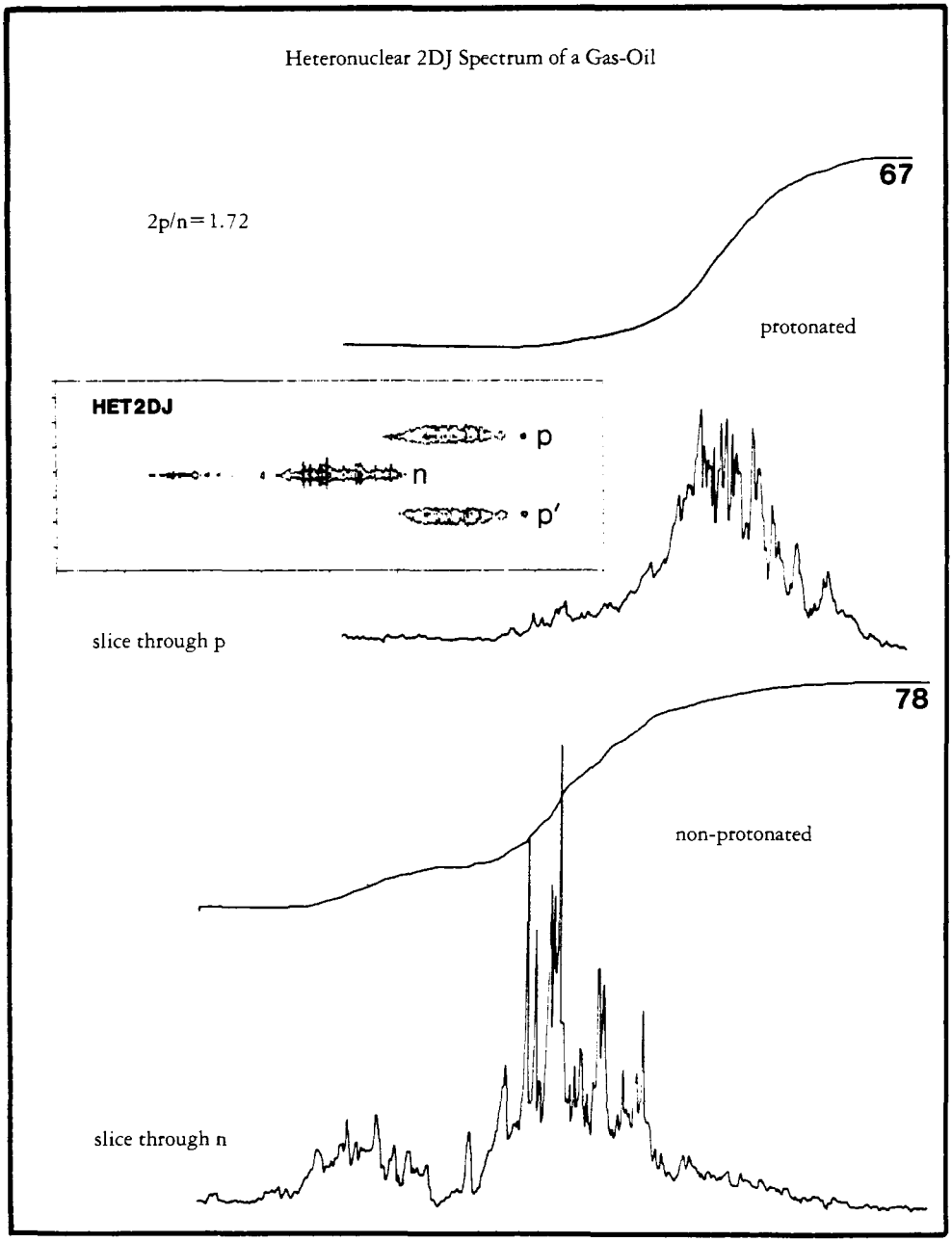

FIGURE 19. Integration of horizontal slices through the data of Figure 18 to give a measure of the CH/C ratio.

A clever use of this experiment has been devised, which allows the effects of proton precession to be observed at the ^{13}C-frequency. It is based on the fact that, after the protons have been reoriented during the free precession period, the magnetization associated with them can be transferred to the ^{13}C-nuclei.

The energy level diagram for a proton and a ^{13}C nucleus that interact by spin-spin coupling is shown in Figure 20a with the Boltzmann populations of the spin states represented by dots. The two ^{13}C transitions and the two proton transitions that give rise to a pair of doublets in each spectrum are labeled according to which nucleus reverses its

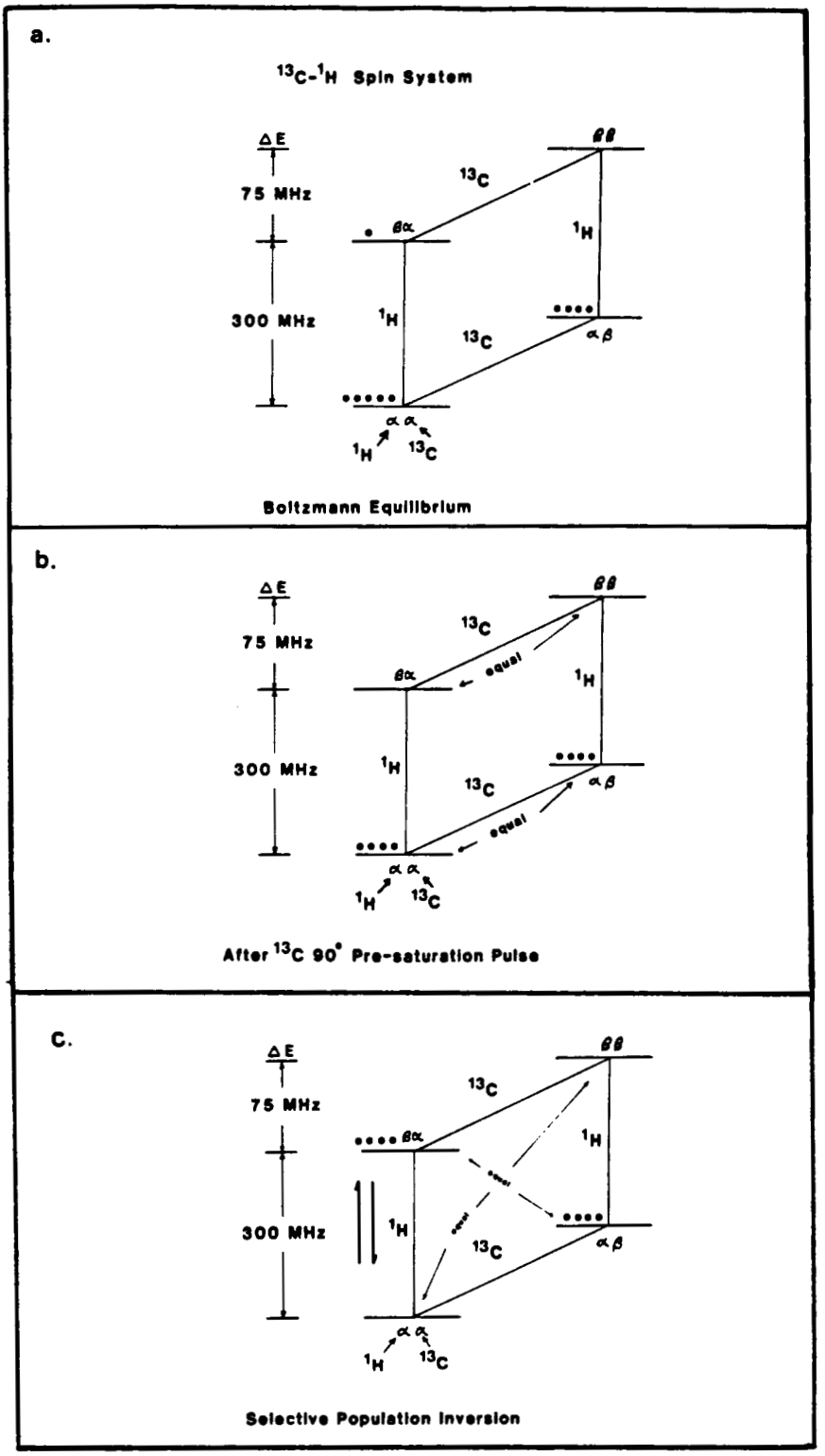

FIGURE 20a. Relative populations of the energy levels of a two-spin (^{13}C-^{1}H) system of nuclei.

FIGURE 20b. Populations after a ^{13}C-90° pre-saturation pulse.

FIGURE 20c. Selective population inversion by the INEPT pulse sequence.

spin. Nuclei aligned with the field have the lower energy and are designated α, while those opposed to the field are β.

After a preparation time of at least three times the longest proton T_1, the proton spin states have essentially reached Boltzmann equilibrium. The ^{13}C-nuclei are usually less effectively relaxed and are in some nonequilibrium state. A reproducible starting point for the experiment can be established by making the z-component of ^{13}C magnetization equal to zero. This is accomplished by a 90° pulse at the ^{13}C-frequency during the preparation time. This "pre-saturation pulse" equalizes the populations in the ^{13}C-energy states and leads to the result shown in Figure 20b.

Consider the following sequence of pulses applied to the sample at the proton- and 13C-frequencies.

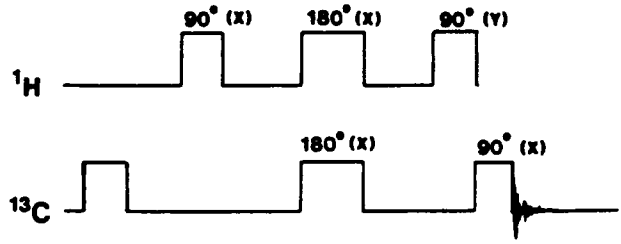

The effect of this sequence is shown in Figure 21. The 90° proton pulse tips the proton magnetization into the xy plane (Figure 21a). During a delay of $1/4J$ sec, the protons bonded to ^{13}C-nuclei with α-spin states precess 90° further than those with the ^{13}C in β-spin states (Figure 21b). At this instant, a 180° proton pulse reorients the proton magnetization vectors around the x-axis (Figure 21c). A simultaneous 180° pulse at the ^{13}C-frequency inverts all of the ^{13}C-spins and thus exchanges the spin labels α and β (Figure 21d). This results in the faster precessing vector being ahead of the slower one, and during the second delay of $1/4J$ sec, the vectors move to opposing positions along the x-axis (Figure 21e). Finally, a 90° proton pulse along the y-axis rotates the proton magnetization arising from protons bonded to carbons with β-spin states back to its equilibrium position along the $+z$ axis. The proton magnetization corresponding to carbons with α-spin states is rotated to the $-z$ axis. This is equivalent to exchanging the populations of the upper and lower energy states βα and ββ in Figure 20b, leading to the situation depicted in Figure 20c.

By applying a 90° pulse at the ^{13}C-frequency immediately after establishing the inverted populations, the intensities of the two lines of the ^{13}C-doublet are changed from their normal value of $+1, +1$ to $+4, -4$. This is due to the fact that the intensity of any nmr line depends upon the population difference of the upper and lower energy states, *i.e.*, the lower minus the upper.

If the proton decoupler is turned on during the ^{13}C-signal acquisition immediately after the polarization transfer, the two magnetization components will precess at the same frequency and their sum (4 minus 4) will give a ^{13}C-line of intensity zero. This is the same result that we would get if we tried to detect ^{13}C-magnetization immediately after the presaturation pulse using normal detection methods. Nothing is gained from the polarization transfer; consequently, the experiment is never performed in that way. Instead, an additional delay before decoupling can be introduced to allow the two lines with intensities $+4$ and -4 to precess at different rates until they have the same phase. This time will vary for CH, CH_2, and CH_3 carbons, just as in the APT experiment, so the one-dimensional polarization transfer experiment (3) (which has been named INEPT[4]) can also be used for spectral editing, *i.e.*, assigning the number of protons attached to each carbon.

[4]Insensitive Nuclei Enhanced by Polarization Transfer.

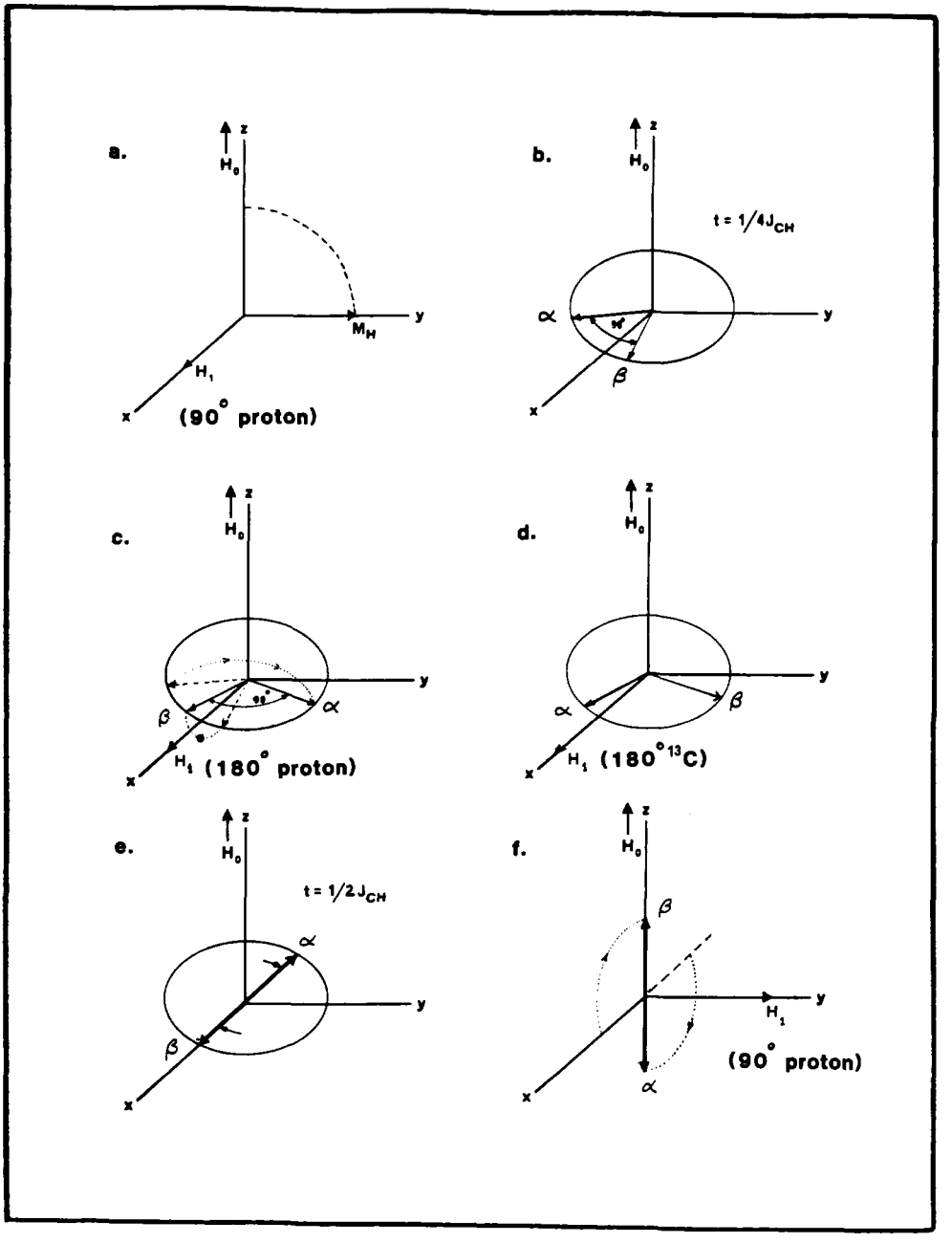

FIGURE 21a. Magnetization vector of the protons bonded to a ^{13}C-nucleus after a 90° pulse.
FIGURE 21b. Divergence of the proton magnetization vectors corresponding to ^{13}C spins in α and β states.
FIGURE 21c. Proton magnetization vectors at time $\tau = 1/4J_{CH}$ after a 180° ^{1}H-pulse along the x-axis.
FIGURE 21d. Reversal of spin labels, α and β, by a 180° ^{13}C-pulse.
FIGURE 21e. Position of proton magnetization at $\tau = 1/2J_{CH}$.
FIGURE 21f. Inversion of populations of protons with ^{13}C in the α state by 90° transfer pulse.

The sum of the intensities of the two lines will be 4+4 or 8 when they have achieved the same phase, so the sensitivity is enhanced four-fold for ^{13}C-nuclei coupled to protons. This is slightly better than the maximum Nuclear Overhauser enhancement of 3. A more significant benefit stems from the fact that the sequence can be repeated as soon

as the protons return to equilibrium via spin-lattice relaxation. The spin-lattice relaxation times, T_1, for protons, are often considerably shorter than those for ^{13}C, so the overall gain in sensitivity can be considerable. For nuclei with smaller magnetic moments and longer T_1 values, such as ^{15}N and ^{29}Si, the gains can be spectacular.

At the time $t = 1/2J_{CH}$, the opposing proton spins shown in Figure 21e are aligned precisely along the x-axis. This alignment, which gives maximum polarization transfer upon application of the 90° proton pulse, is independent of the proton chemical shift. This is true only at the instant $\tau = 1/2J$ due to the refocusing effect of the 180° proton pulse. At all other times, the alignment of the spins will be dependent on the chemical shift as well as the value of J_{CH}.

Far from being a nuisance, this chemical shift dependence can be turned to good use. If a brief additional delay, Δt, were introduced between the time $t = 1/2J$ and the application of the proton polarization transfer pulse, the opposed vectors of Figure 21e will rotate an additional amount $\Delta t\ \delta_H \omega_0$, where δ_H is the proton chemical shift in parts per million relative to the pulse frequency. Only the component of α and β along the x-axis will be rotated back to the z-axis by the proton 90° (y) pulse. Thus the amplitude of the ^{13}C signals becomes modulated at the proton chemical shift frequency as the value of Δt is varied. The sequence of events up to $t = 1/2J$ can be considered the preparation time, Δt the evolution time, and the period following the polarization transfer pulse and the ^{13}C-90° pulse, the acquisition time. Many spectra with increasing values of Δt can be aligned in a data matrix to yield a 2D plot showing the correlation of proton and carbon chemical shifts.

In the actual heteronuclear correlation 2D experiment (often called HETCOR), it is not necessary to refocus the proton chemical shifts because their effect on the ^{13}C-intensities is the whole purpose of the experiment. The 180° proton pulse can, therefore, be omitted.

The C-H coupling constant, J_{CH}, determines the timing of the sequence. This leads to two versions of the experiment with very different significance in structure determination. The first version, direct or one-bond HETCOR, requires a J_{CH} between 125 and 160 Hz, depending on whether the CH correlations being observed arise from sp^3 or sp^2 carbons. This experiment identifies the bonding of protons (represented by spectral peaks or multiplets in the proton spectrum) to each carbon in the ^{13}C-spectrum. In the case of ethyl alcohol, an idealized contour plot of the data would have the appearance of Figure 22a.

The second, and perhaps more valuable version, long-range HETCOR, requires a J_{CH} between 5-10 Hz, an average of 7 Hz being a good compromise. For two-bond and three-bond couplings that are not exactly equal to 7 Hz, some sensitivity is lost. However, the polarization transfer is a slowly changing function of J_{CH}, and most couplings will be picked up. This experiment identifies which proton peaks should be assigned to the protons on carbons adjacent to or once more removed from the carbon being observed. In the case of ethyl alcohol, an idealized contour plot would look like Figure 22b.

An example of the power of the HETCOR experiment in choosing between structural alternatives is shown in Figure 23. Structures **1** and **2** differ only in the arrangement of the *gem*-dimethyl groups and cannot be distinguished from each other by analysis of their ^{1}H- and ^{13}C-nmr spectra. A coupled ^{13}C-spectrum showing the long-range couplings to the quaternary carbon *c* would solve this problem in principle, but even the most powerful modern instrumentation failed to give an unequivocal result. The HETCOR plot showing the carbons and protons coupled through two or three bonds gives an unambiguous answer to the question. The spiro carbon (**c**) in Figure 23 shows correlations to all four of the *gem*-methyls and therefore must be located between car-

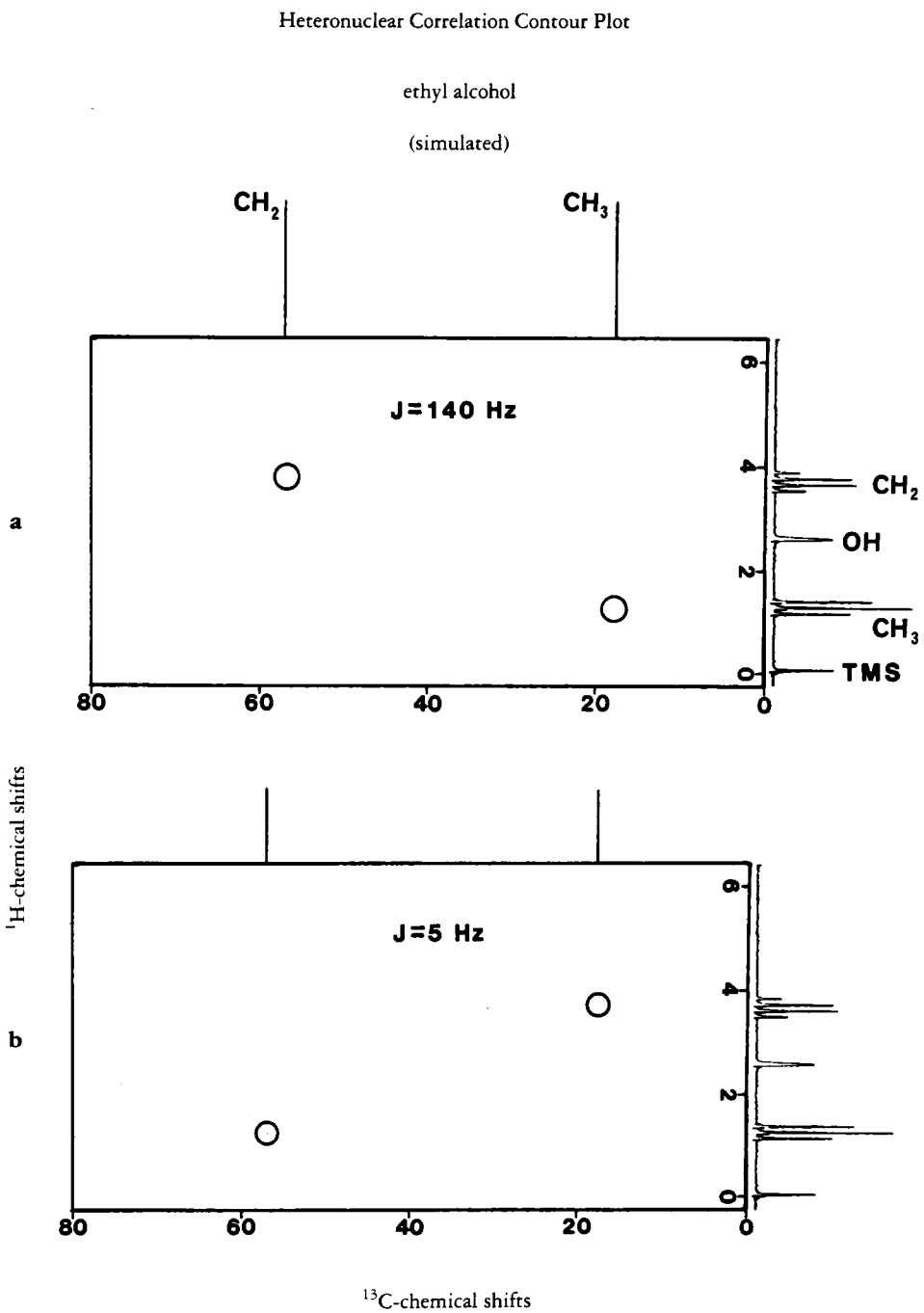

FIGURE 22a. Simulated heteronuclear one-bond correlation plot for ethyl alcohol.
FIGURE 22b. Simulated long-range heteronuclear correlation plot for ethyl alcohol.

bons **a** and **b**. Coupling through four bonds would be required for two of the methyls in structure **2**. Four bond couplings are too small to be observed in this experiment.

THE CARBON-CARBON CONNECTIVITY NMR EXPERIMENT.—Two carbon atoms that are joined by a chemical bond exhibit spin-spin coupling if both of the atoms contain a ^{13}C-nucleus. Due to the one percent abundance of ^{13}C, only one molecule in ten thousand exhibits coupling. Detection of the pairs of ^{13}C-doublets that exist for each

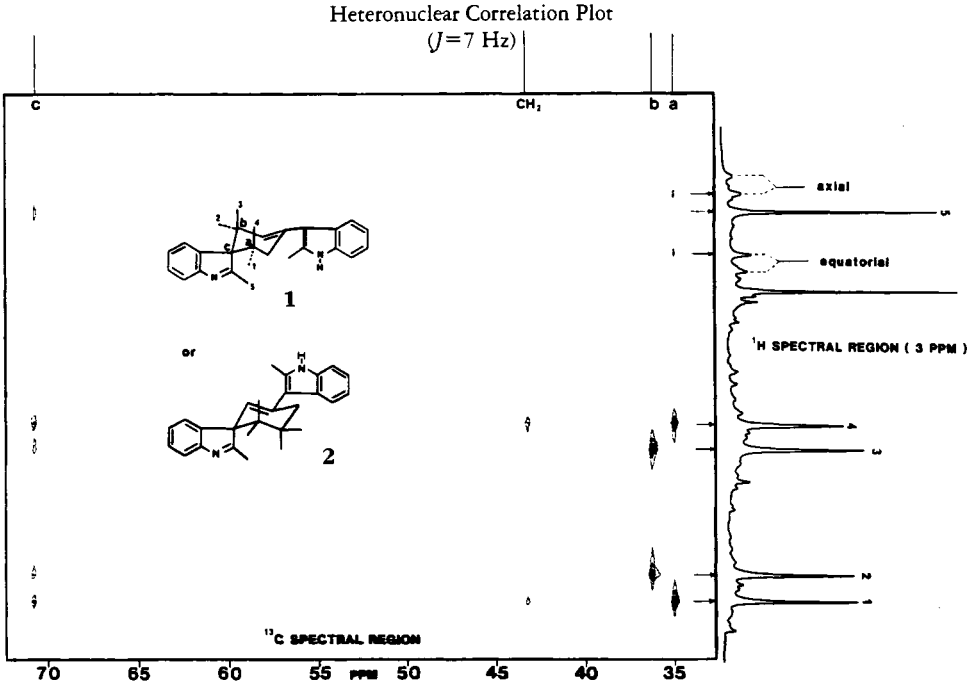

FIGURE 23. Heteronuclear correlation plot for the methyl protons and the spiro-carbon in a complex organic compound.

carbon-carbon bond in the molecule is extremely difficult because of the presence of singlet lines one hundred times more intense. These arise from molecules with only one ^{13}C-nucleus and, except for a small isotope effect, fall at nearly the same chemical shift.

A unique property of a coupled spin system can be employed to differentiate between the singlets due to the mono-isotopic molecules and the doublets due to the coupled spin solvent. This property is called "double quantum coherence" and is possible only in two-spin systems in which the nuclei interact in such a way that they share common energy levels.

A pulse sequence has been developed (4,5) which is capable of converting the two-spin system of bonded ^{13}C-nuclei to the state of double quantum coherence.

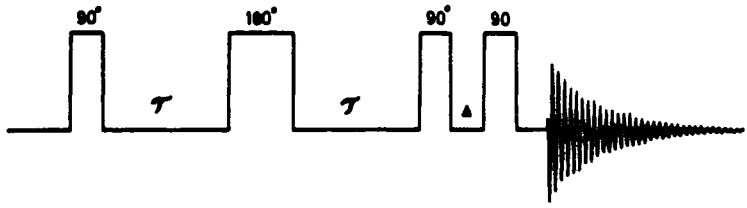

At the very special time $\tau = 1/4J_{CC}$, all of the coupled pairs of ^{13}C-nuclei precessing about H_0 momentarily come into phase coherence along the x-axis. At this instant, the third pulse is applied along the x-axis and creates double quantum coherence. This rearrangement of the nuclear spins initiates an evolution of phase relationships. This, in turn, allows conversion of double quantum coherence back into magnetization precessing in the xy plane at a later time. The conversion to double quantum coherence and back again introduces a phase shift in the signals. The pairs of doublets due to the bonded carbons are then distinguishable from the unwanted intense signals due to the ordinary ^{13}C-species. Figure 24 shows the resulting spectrum for a complex molecule when the fourth pulse follows the third with a delay, Δ, of 10 μsec.

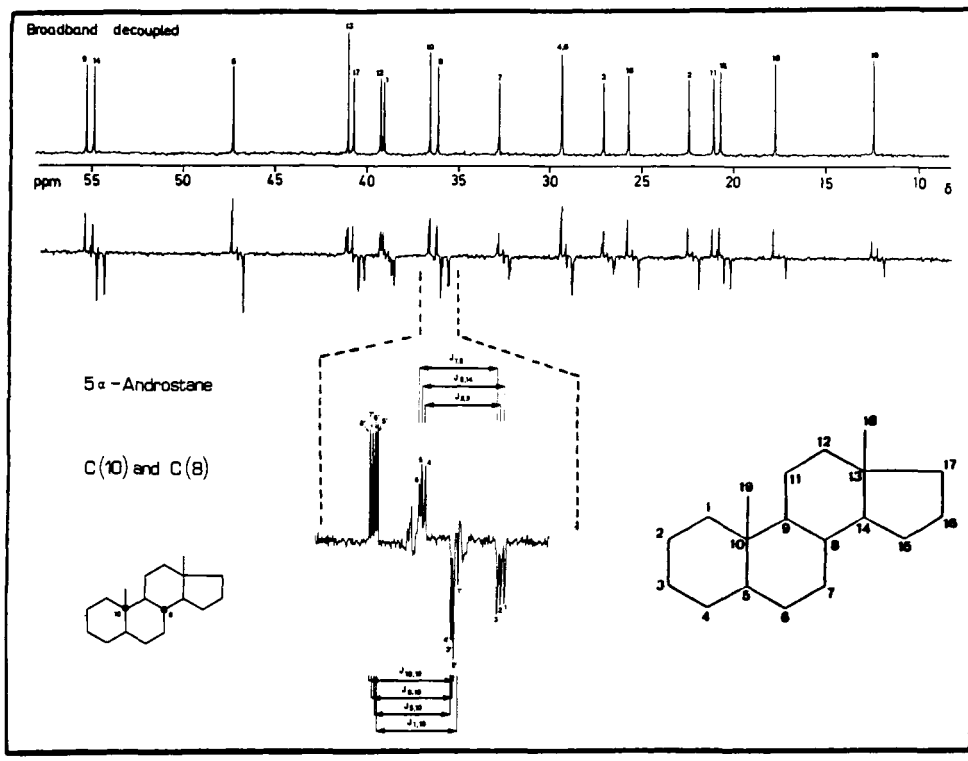

FIGURE 24. Broadband decoupled spectrum of 5α-androstane with corresponding ^{13}C-^{13}C satellite spectrum and expanded region showing ^{13}C-doublets from carbons 8 and 10.

The one-dimensional display of the ^{13}C-^{13}C couplings can be very difficult to interpret because of the severe overlapping of the doublets as an expansion of the signals from carbons 8 and 10 in Figure 24 illustrates. By the use of resolution enhancement techniques, it is possible to resolve the various couplings. The low abundance of the doubly labeled ^{13}C-species requires the use of concentrated samples to overcome the loss in sensitivity, and such solutions are not always conducive to high resolution. Even if the resolution can be achieved, accidental overlap of the doublets may prevent successful spectral analysis.

The obvious solution to this difficulty is to spread the information into two dimensions by allowing the double quantum coherence to evolve before detecting the ^{13}C-signals (6). If the time period designated Δ in the pulse sequence is incremented to produce a series of spectra, a 2D display can be generated that will show each pair of doublets from bonded carbon atoms shifted into the second dimension by an amount corresponding to the double quantum frequency of the coupled spin system. Only the bonded carbons share a common double quantum frequency so that identification becomes trivial.

Figure 25 shows a 2D representation of the data found in a one-dimensional carbon-carbon connectivity plot for androstane. Instead of piling up along a single axis, each pair of doublets lies on a separate horizontal line at the double quantum frequency for the coupled nuclei. The double quantum frequency is proportional to the average of the chemical shifts in this experiment; consequently, all of the pairs of doublets are symmetrical about a single diagonal line. This constraint aids in distinguishing real signals from artifacts.

If the display of Figure 25 were viewed from above, the plot would be rectangular, and the peaks would appear as circles or spots. This form of display, called a contour

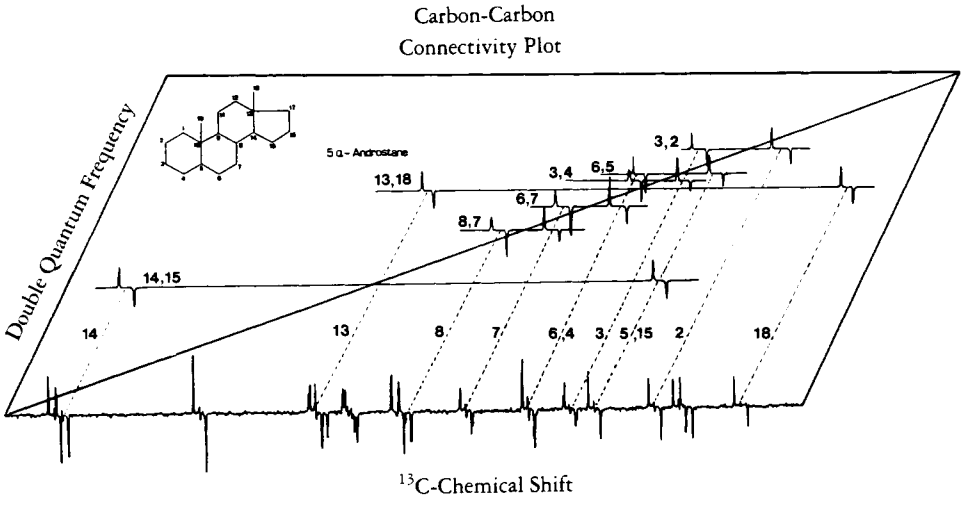

FIGURE 25. Perspective view of CCC2D plot.

plot, is the most common way to present the data. Figure 26 shows a contour plot of a 75 MHz carbon-carbon connectivity 2D (CCC2D) data set for the sesquiterpene cedrol, $C_{15}H_{26}O$. The normal broadband decoupled spectrum is plotted at the top of the chart, along with the multiplicities determined by the APT technique. Peaks are numbered 1-15 consecutively from left to right. All of the chemical bonds can be established from the one experiment, and the structural formula follows directly. Stereochemistry is not elucidated by the connectivity data and must be determined by other methods.

STRUCTURE OF AN UNKNOWN COMPOUND USING CCC2D AND LONG RANGE HETCOR.—When hetero-atoms (O, N, S, etc.) are present, not all of the bonds can be established from carbon-carbon connectivity data. Furthermore, unless 1 ml of a 1.0-M solution is available, it may not be possible to observe all of the pairs of signals needed to establish the structure. In such cases, combining the data from two separate 2D nmr experiments can facilitate progress and possibly lead to a complete structure.

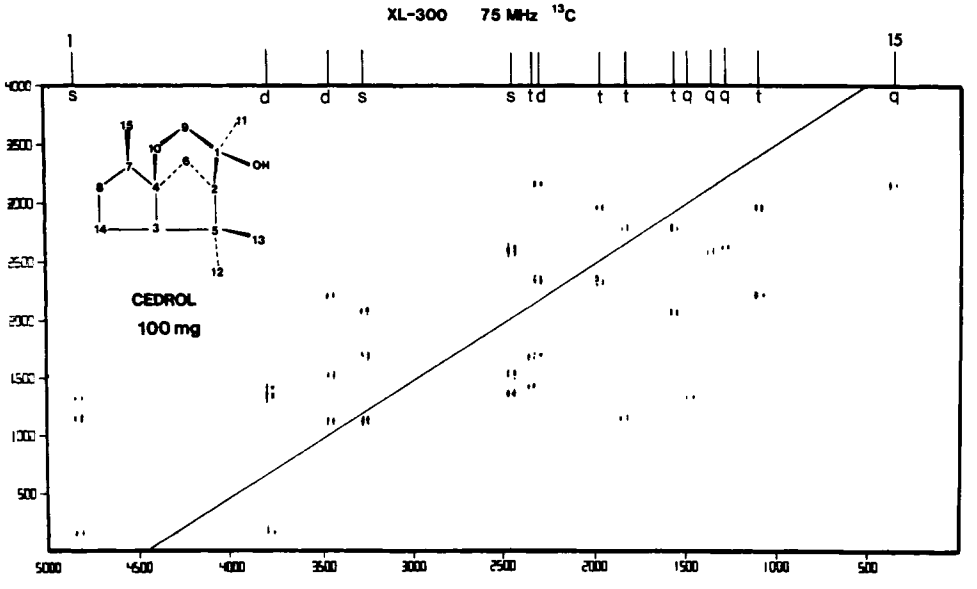

FIGURE 26. CCC2D plot for cedrol.

A compound was shown by ^{13}C-nmr to contain two methyl groups, one methoxyl, one CH group, and five nonprotonated carbons. Its proton spectrum showed no spin-spin couplings, and, in addition to the methyl peaks and the CH peak, it showed a sharp line due to one proton at 18.4 ppm. The carbon-carbon connectivity plot, shown in Figure 27a, allowed the following bonds to be established:

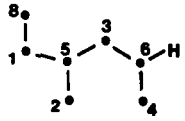

Figure 27b shows the long-range HETCOR data for the same compound. Carbon 3 shows a strong correlation to the methoxyl protons, while 2 and 4 both correlate to the methyl protons at 3.36 ppm. Therefore, three-bond paths must connect the same methyl protons to both carbons 2 and 4, requiring the placement of the nitrogen to close the ring (**3**):

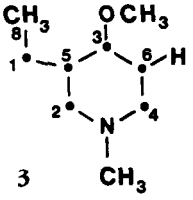

3

The remaining three oxygen atoms and the proton at 18.4 ppm are accommodated by adding two carbonyl oxygens and an enolic OH group as shown below (**4**):

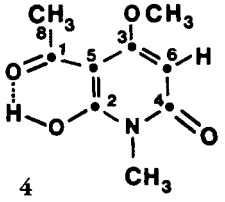

4

The enolic proton forming a six-membered ring in a strong hydrogen bond accounts for the 18.4 ppm proton shift, while the ^{13}C-chemical shifts of carbons 1, 2, and 4 are in accord with this structure.

It is interesting to note that carbon 1 at 191 ppm shows correlations to the methyl protons at 2.57 ppm as expected and, unexpectedly, to the enolic proton. The enolic proton also shows a correlation to carbon 2, and to the methyl carbon, 8. If the hydrogen bond is truly ionic, no correlation to 1 should be observed. However, if the compound is a hybrid of structures **5** and **6** as many chemists would expect, the observations are explained.

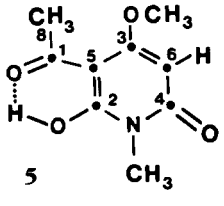

5

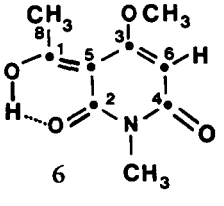

6

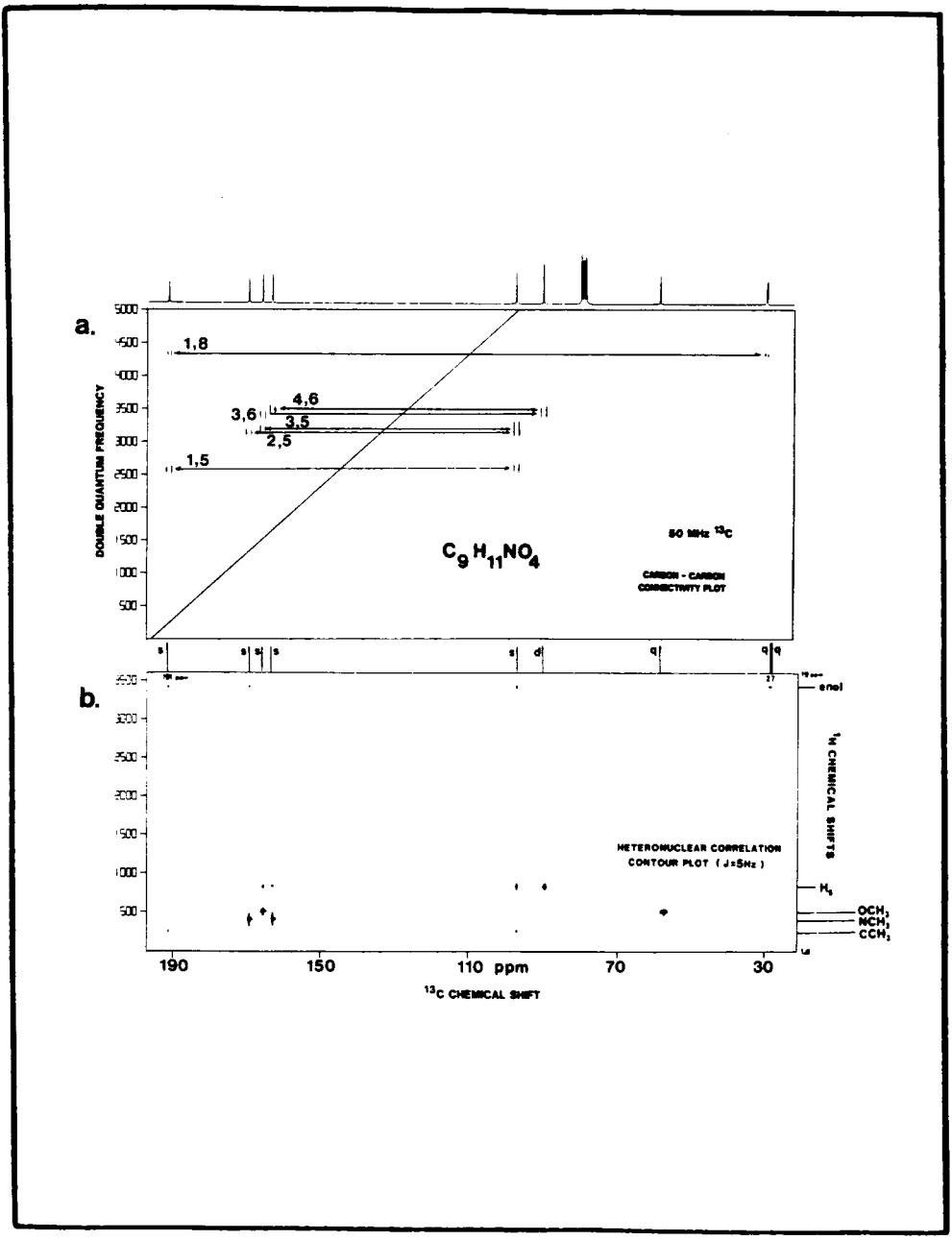

FIGURE 27a. CCC2D plot for $C_9H_{11}NO_4$.
FIGURE 27b. Long-range HETCOR plot for $C_9H_{11}NO_4$.

DEVELOPMENTS IN PROTON NMR.—The developments in proton nmr are no less impressive than in ^{13}C-nmr. Superconducting magnets have made proton resonance frequencies in the vicinity of 300 MHz commonplace, and 400 MHz is rapidly moving into the same category. Frequencies of 500 MHz are beginning to appear, and at least one 600 MHz spectrometer is operating on a regular basis.

In addition to the great improvement in sensitivity, the spectral dispersion in proton nmr has increased proportionately to the magnetic field strength. The greater field strength increases the chemical shifts without affecting spin-spin couplings, thereby

reducing the chance of overlap of the spectral multiplets. This often results in a first-order appearance of the splitting patterns.

Interpretation of proton spin-spin coupling patterns has, until recently, depended heavily upon homonuclear spin decoupling. Unfortunately, instrumental artifacts sometimes give rise to misleading interpretations. While homonuclear decoupling is by no means obsolete at this point, the 2D nmr experiment called homonuclear correlation spectroscopy (HOMCOR or COSY) often gives better, more uneqivocal results. A single HOMCOR experiment, by displaying all of the proton-proton spin couplings on one 2D plot, can replace a great many homonuclear decoupling experiments.

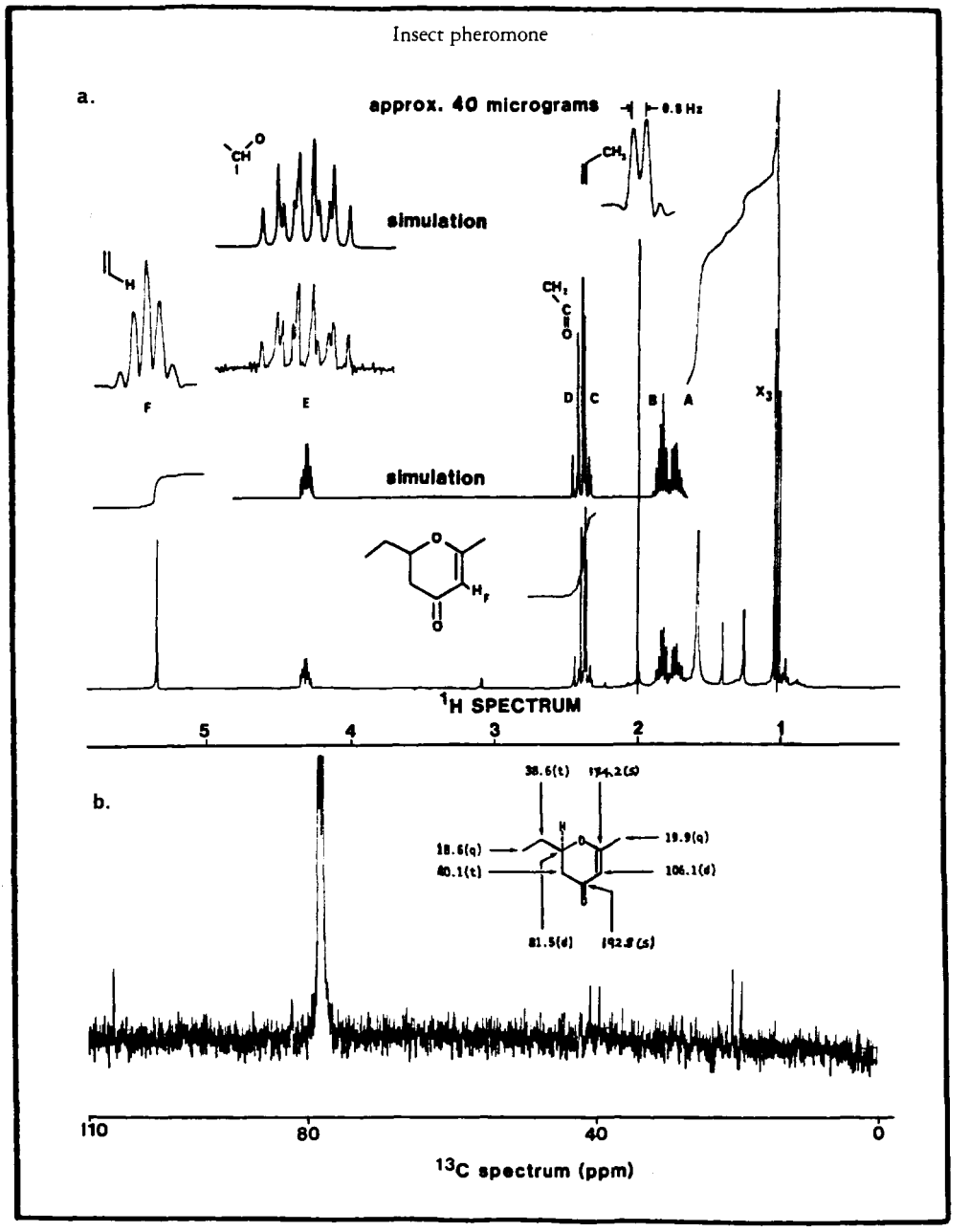

FIGURE 28a. Proton 400 MHz spectrum of an insect pheromone with simulation of the spectrum.
FIGURE 28b. ^{13}C-spectrum of the same sample.

STRUCTURE OF AN INSECT PHEROMONE.—A sample of a substance extracted from the hairpencils of the male moth *Hepialus californicus* B. was submitted for nmr analysis. Although alleged to weigh about 1 mg, the sample was totally invisible, and even after overnight data acquisition displayed only six extremely weak ^{13}C-spectral lines. The sample size was later estimated to be about 40 μg.

The ^{1}H-spectrum at 400 MHz was, however, clear and simple and could be simulated as an $ABCDEX_3$ spin system. Figure 28a shows a methyl triplet and nonequivalent methylene coupled to it (J=7.5 Hz), with the methylene protons also exhibiting coupling (J=5.5, 7.5 Hz) to the proton at 4.31 ppm. This CH group is presumed to be adjacent to an oxygen on the basis of its chemical shift. A methyl at 2.00 ppm shows a 0.8 Hz coupling to a vinylic proton at 5.34, suggesting a *cis*-configuration of the vinylic proton and the methyl. A second nonequivalent CH_2 group at 2.35 and 2.42 ppm exhibits a 13.5 Hz coupling between one of the CH_2 protons and the CH adjacent to the oxygen. Such a large coupling is diagnostic of an axial-axial arrangement of protons in a six-membered ring.

The proton results indicate that the ^{13}C-spectral lines are authentic (Figure 28b). The shift of 106.0 ppm for the protonated vinylic carbon suggests that the oxygen is linked to the other vinylic carbon. The six-membered ring must be completed with a nonprotonated carbon, and the ^{1}H- and ^{13}C-chemical shifts of the adjacent CH group are compatible with a carbonyl carbon in this position. Long-range "W"-type coupling between the vinylic proton and the equatorial proton of the CH_2 group at 2.35 ppm also supports this structure.

Accordingly, the substituted dihydropyranone structure (7) shown below was proposed.

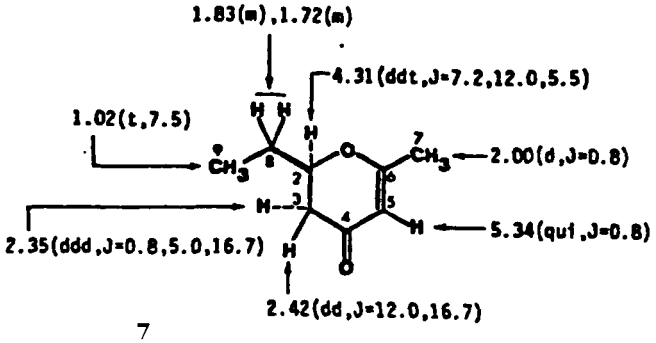

7

The compound was synthesized, and its ^{1}H- and ^{13}C-nmr parameters as well as ir, uv, and ms were identical to the natural product. Later cd studies established the absolute configuration of the compound as (2-*R*)- 2,3-dihydro-2-ethyl-6-methyl-4H-pyran-4-one. It has been named hepialone (7).

ASSIGNMENT OF COMPLEX ^{1}H-SPECTRUM BY HOMONUCLEAR CORRELATION SPECTROSCOPY.—A very simple pulse sequence that makes it possible to correlate the chemical shifts of protons whose spins are coupled is shown below.

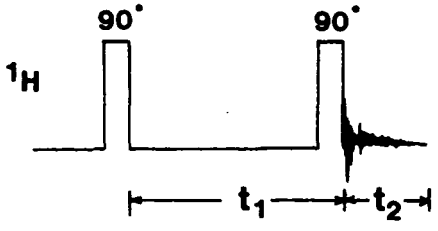

As usual, the data acquired during t_2 represent the chemical shifts in the ^{1}H-spectrum. As the time t_1 is incremented, the intensities of the proton peaks vary at the frequency of the peaks themselves and at the frequency of other protons sharing common energy levels, *i.e.*, protons coupled to the one being observed. Two-dimensional data processing results in a HOMCOR contour plot display of the type shown in Figure 29. Both dimensions of the plot represent the proton spectrum, with the spectral peaks falling on the diagonal. Off-diagonal peaks appear in symmetrical positions and denote coupling between the two protons represented by the peaks at the corresponding positions on the diagonal.

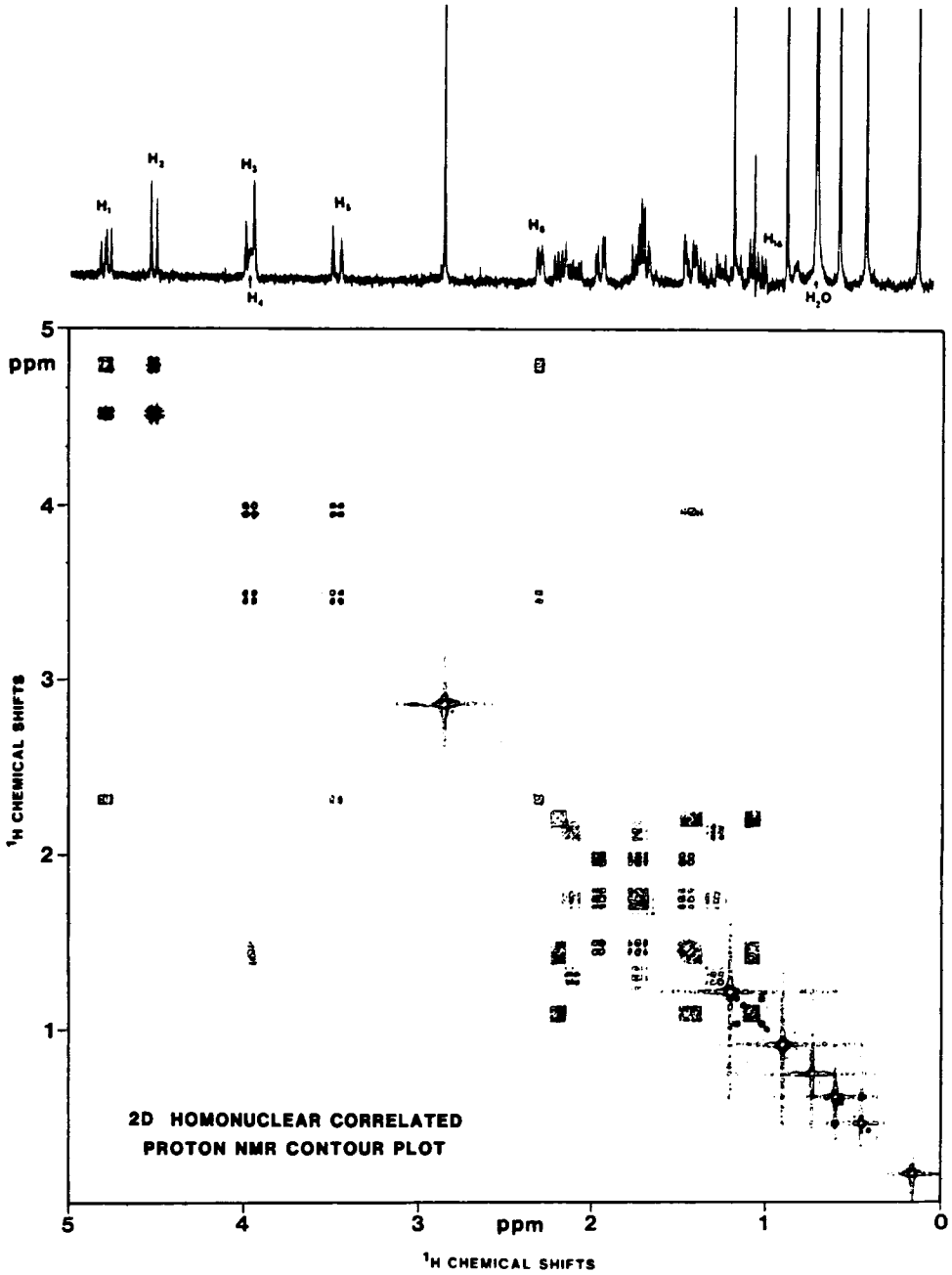

FIGURE 29. Proton homonuclear correlation 2D contour plot.

The compound whose HOMCOR plot is shown in Figure 29 contains ten protons whose multiplet ^{1}H-resonances fall in a 400 Hz range (1.33 ppm). A plot expansion for the protons 6-16 is displayed in Figure 30. The HOMCOR plot reveals the source of the couplings contributing to each multiplet. Matching the peak spacings shared by the nonequivalent protons allows the Table of Coupling Constants in Figure 30 to be constructed. Thus, 2D techniques can simplify the traditional laborious series of decoupling experiments formerly needed to extract this information.

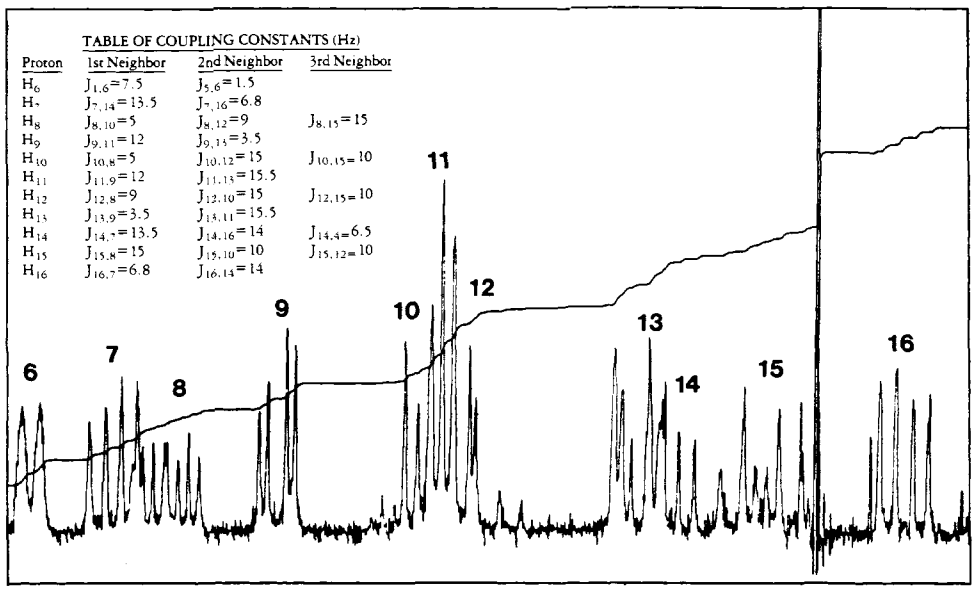

FIGURE 30. Complex ^{1}H-spectral region for the compound in Figure 29 with a Table of Coupling Constants deduced with the aid of the 2D data.

STRUCTURE OF AN INSECT GROWTH INHIBITOR FROM MARINE ALGAE.—A biologically active compound (with the proposed structure **8** based on mass spectral data) was subjected to ^{1}H-nmr analysis at 300 MHz and ^{13}C-nmr analysis at 75 MHz. The absence of a vinyl group and the presence of a CH_2-OH group could be demonstrated, leading to proposed structures **9** and **10**.

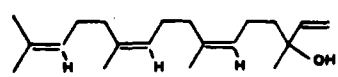

8

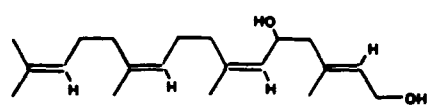

9

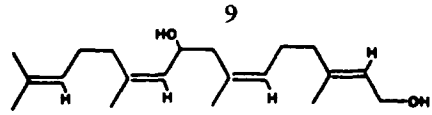

10

A distinction between these alternatives could not be drawn from the one-dimensional nmr spectra, but the HOMCOR plot of Figure 31 contains the essential information needed to complete the structure elucidation.

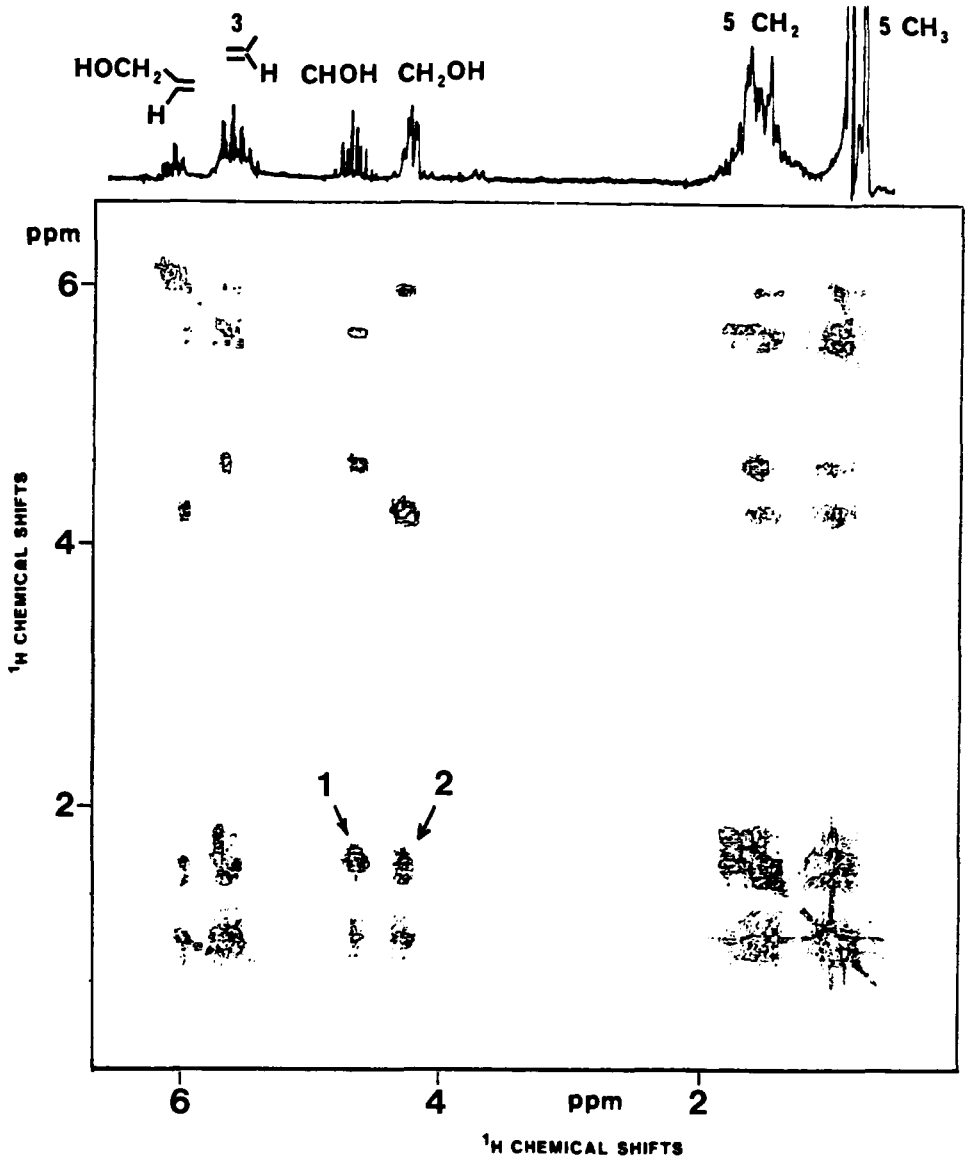

FIGURE 31. ^{1}H-HOMCOR plot for an insect growth inhibitor from marine algae.

Spin-spin coupling from the CH_2OH to the CH_2 protons at C_4 will be observed through five bonds in either compound **9** or **10**. The CHOH proton will couple its spin through three bonds to the CH_2 protons at C_4 in the 5-hydroxy compound (**9**) and to the CH_2 protons at C_8 in the 9-hydroxy compound (**10**). The two correlations designated 1 and 2 on the HOMCOR plot confirm the existence of the predicted couplings. From their different appearance and different location on the plot, it is clear that the CHOH and CH_2OH protons couple to different CH_2 groups. Therefore, structure **9** cannot be correct, and the compound is shown to be the 9-hydroxy compound, **10** (8).

CONCLUSION.—Of the many recent improvements in nmr, the 2D techniques seem to have the greatest potential for increasing the chemist's ability to solve difficult structural problems. New experiments are being devised at frequent intervals, and the probability of even more selective and more useful pulse sequences is high. During the

next decade natural products chemists are likely to see the value of nmr extended as far beyond its present state as the methods described in this survey go beyond traditional one-dimensional techniques.

LITERATURE CITED

1. D.L. Rabenstein and T.T. Nakashima, *Anal. Chem.*. **51**, 1465A (1979).
2. S.L. Patt and J.N. Shoolery, *J. Magn. Reson.*. **46**, 535 (1982).
3. G.A. Morris and R. Freeman, *J. Am. Chem. Soc.*. **101**, 760 (1979).
4. A. Bax, R. Freeman, and S.P. Kempsell, *J. Am. Chem. Soc.*. **102**, 4849 (1980).
5. A. Bax, R. Freeman, and T.A. Frenkiel, *J. Am. Chem. Soc.*. **103**, 2102 (1981).
6. A. Bax, R. Freeman, and T.A. Frenkiel, *J. Magn. Reson.*. **43**, 478 (1981).
7. I. Kubo, T. Matsumoto, D.L. Wagner, and J.L. Shoolery, *J. Am. Chem. Soc.* (in press).
8. I. Kubo, T. Matsumoto, N. Ichikawa, and J.N. Shoolery (to be published).